http://www.ijps.in
e-ISSN: 2455-6270 p-ISSN: 2455-7455

N=1/F-Theory Resolutions

Deep Bhattacharjee *
DOI: 10.37648/ijps.v21i01.022
Received: 12/05/2026; Accepted: 01/06/2026; Published: 03/06/2026

This paper develops a compact framework for four-dimensional $N = 1$ F-theory on resolved elliptic Calabi–Yau fourfolds. The discussion starts from the Weierstrass model, keeps track of crepant resolution data, and follows the same classes through the Shioda map, the shifted G_4-flux law, tadpole cancellation, matter-surface indices, and residue formulae for holomorphic Yukawa couplings. The main point is that these calculations can be placed in one clean sequence of lattice, Chow-ring, and Deligne-cohomology steps. Within the stated admissible class, the flux set is finite, chiral indices are integral, hypercharge masslessness becomes a lattice condition, and local Yukawa entries reduce to finite residue algebra. The paper also gives worked $SU(5)$, $SO(10)$, Pati–Salam, E_6, and abelian-sector computations with diagrams and full reference data.

I. INTRODUCTION AND STATEMENT OF UNRESOLVED PROBLEMS

Related background for this part is compared with the author's work in [22].

[2] The past two decades have witnessed remarkable progress in the geometric engineering of four-dimensional $\mathcal{N} = 1$ supersymmetric quantum field theories via F-theory compactified on elliptically fibered Calabi–Yau fourfolds [1–4]. The basic paradigm is well established: choose a smooth base threefold B_3 with effective anti-canonical bundle, construct a Weierstrass model Y_4 with sections $f \in H^0(B_3, \mathcal{O}(-4K_B))$ and $g \in H^0(B_3, \mathcal{O}(-6K_B))$, resolve the singularities to obtain a crepant resolution $\widehat{Y}_4$, and turn on a self-dual four-form flux $G_4 \in H^{2,2}_{\mathbb{Z}}(\widehat{Y}_4)$ subject to a shifted quantization law, transversality constraints, and a D3-tadpole cancellation condition. The effective field theory is then read off from the intersection theory of the resolved geometry and the zero-mode spectrum of the Dirac operator on matter surfaces. Despite the immense number of concrete models constructed and the successful engineering of many features of the Minimal Supersymmetric Standard Model (MSSM), several foundational aspects have remained either partially understood or entirely unresolved.

The purpose of this paper is to put these gaps into a single set of precise geometric problems and to solve the parts that are determined by the stated compact data. We construct a *twisted Deligne hypercohomology* tailored to the half-integral shift of G_4 and the Freed-Witten anomaly, a *motivic scanning lattice* that underlies the finiteness of flux vacua and allows finite enumeration, a *derived category method* for computing the full vector-like spectrum (not merely the net chirality), an *excision calculus* for non-flat fibers, and a *residue Hodge theory* that explains the rank and texture of holomorphic Yukawa couplings. Equipped with these tools, we give proofs, within the stated admissible class, for the following standard technical questions:

(P1) **Precise flux quantization and Deligne lift:** The standard statement $G_4 + \frac{1}{2}c_2(\widehat{Y}_4) \in H^4(\widehat{Y}_4, \mathbb{Z})$ is insufficient to capture the flat gerbe part needed for the vector-like zero modes. We construct a Deligne cohomology with a twisted differential that naturally encodes the shift.

(P2) **Resolution of all singular fibers (non-flat contributions):** Codimension-two and -three loci often have fiber dimension jumps that are not flat limits of the elliptic fibration. We develop an algebraic excision procedure that replaces any non-flat component by a flat small resolution and proves that the chiral index is unchanged.

(P3) **Controlled moduli stabilization:** While complex structure moduli are fixed by the Gukov-Vafa-Witten superpotential $\int G_4 \wedge \Omega_4$, the Kähler moduli often remain flat or are only partially fixed by non-perturbative effects. We give explicit sufficient conditions under which the non-perturbative superpotential fixes the Kähler moduli, and the admissible flux choices remain finite under the tadpole bound.

(P4) **Massless hypercharge and swampland constraints:** The condition $\pi_*(G_Y \cdot D_a) = 0$ for a massless $U(1)_Y$ gauge boson must be compatible with chirality and tadpole cancellation. We reduce the compatibility problem to a finite Diophantine system on each chosen base.

(P5) **Global gauge group structure:** The actual gauge group is not simply connected; it involves the Mordell–Weil group, its torsion, and the Tate–Shafarevich group. We give an algorithm to compute the global gauge

* Corresponding author: Deep Bhattacharjee; Electro-Gravitational Space Propulsion Laboratory (EGSPL), Bhubaneswar, Odisha, India; ORCID: 0000-0003-0466-750X; Email: d.bhattacharjee@erl-forschung.de.

[1] How To Cite The Article: Bhattacharjee D.; (June 2026) *N=1/F-Theory Resolutions*; International Journal of Professional Studies; Jan–Jun 2026, Vol. 21, pp. 945–982; DOI: 10.37648/ijps.v21i01.022.

[2] The surrounding Calabi–Yau and conjectural-background literature by the author is cited only as programme context [5, 10, 13, 19, 25].

group and all discrete symmetries.

(P6) **Vector-like zero modes and Yukawa rank:** The net chirality is only the index of a Dirac operator; the full zero-mode count depends on the Deligne lift of G_4. We compute the vector-like pairs via a derived category pushforward. Moreover, the rank of the holomorphic Yukawa matrix, which often is one, is derived from the spectral invariants of the local residue ring.

(P7) **Landscape finiteness:** We rigorously prove that the number of physically distinct flux vacua on a compact Calabi–Yau fourfold is finite, using the positive definiteness of the Hodge inner product on primitive vertical cycles.

All these results are obtained within the framework of an *admissible compact datum*, which we define precisely in Section II. Our proofs are constructive and algorithmic; they can be implemented in computer algebra systems. To demonstrate the power of the framework, we work out fully detailed examples for $SU(5)$ and $SO(10)$ Grand Unified Theories in Sections IX and X. Further, we extend the analysis to E_6 models, discuss the swampland constraints in depth, and provide a complete duality map with heterotic compactifications.

The paper is organized into two parts. Part I (Sections II–VIII) introduces the new constructions and proves the theorems that resolve the above problems. Part II (Sections IX–XIV) applies these tools to explicit compact models, presenting Groebner basis reductions, flux tables, finite vacuum counts, and 3D visualizations of the tadpole ellipsoid. Appendices collect computational data, and a user guide for our software implementation. Footnotes explain the geometric points that are easy to misread, and the diagrams are used only where they clarify the calculation. The presentation is self-contained: all necessary results from intersection theory, Hodge theory, and derived categories are recalled, and new proofs are given for any statement that does not already appear in the standard F-theory literature.

A. Historical context and the need for new mathematics

The F-theory approach to particle physics [48, 49, 81] has produced a remarkably successful set of local and global GUT models. However, a precise formulation of the flux background as a fully quantum consistent object has been missing. The standard flux G_4 is treated as a class in $H^{2,2}(\widehat{Y}_4) \cap H^4(\widehat{Y}_4, \mathbb{Z})$, but the K-theoretic and M-theoretic origins indicate that the C-field is an element of a differential cohomology theory that reduces to Deligne cohomology in the large volume limit [32, 33, 38]. The half-integral shift $G_4 + \frac{1}{2}c_2(\widehat{Y}_4)$ is a consequence of the Freed-Witten anomaly for D3-branes wrapping curves in the fourfold. In Deligne cohomology, this shift is built in via a twisted differential, and the flat part (the intermediate Jacobian) controls the vector-like pairs and the theta angles of the gauge theory. Our construction of *twisted Deligne hypercohomology* in Section III resolves problem (P1) by giving a functorial definition of the flux lattice that includes both the topological class and the flat gerbe data.

Problem (P2) on non-flat fibers has been a persistent source of confusion. The standard matter surface S_R is defined as the fibration over a matter curve C_R inside the discriminant, but at points where the vanishing orders of (f, g, Δ) jump, the fiber dimension can become two or three, leading to a surface that is not equidimensional over the base. Physicists have often simply ignored these non-flat components, arguing that they do not contribute to chirality, but a rigorous justification was missing. Using an algebraic excision technique inspired by Grothendieck's local cohomology and deformation theory, we show that any non-flat fiber can be replaced by a flat small resolution whose total contribution to the index and tadpole is precisely the same as the naive calculation that throws away the non-flat part (Section VII). This provides the long-sought mathematical foundation for the practice.

Problem (P3) on controlled moduli stabilization is perhaps the most important for phenomenological applications. The flux superpotential $W_{\text{flux}} = \int_{\widehat{Y}_4} G_4 \wedge \Omega_4$ generically fixes all complex structure moduli because the number of flux degrees of freedom exceeds $h^{3,1}$ by a large margin. However, Kähler moduli appear in the no-scale potential at tree level and only acquire a potential via non-perturbative corrections (Euclidean D3-branes or gaugino condensation) and α' corrections. It has been an open question whether for a *given* compact fourfold and a *given* flux, a non-perturbative superpotential can be generated that fixes all Kähler moduli in a controlled regime. Our analysis in Section V uses the motivic scanning lattice to prove that one can always adjust the flux integers (within the tadpole ellipsoid) so that the resulting W_0 falls into the region of parameter space where the complete stabilization exists. Moreover, we show that the number of such vacua is finite and explicitly bounded.

Problems (P4) and (P5) on hypercharge masslessness and global gauge group are tackled by a combined use of Shioda maps, height pairings, and the Mordell–Weil lattice. We solve the linear Diophantine equations for the flux coefficients whenever the associated Smith normal form has a compatible integral right-hand side. The global gauge group, including all discrete symmetries, is computed algorithmically from the resolution data; we illustrate the procedure for $SU(5)$ and $SO(10)$ models, obtaining, for instance, the gauge group $Spin(10)/\mathbb{Z}_4 \times U(1)$ in a model with an extra rational section.

Problem (P6) on vector-like zero modes and Yukawa rank is the most subtle, as it goes beyond the index theorem. The chiral index χ_R counts the difference between the numbers of chiral and anti-chiral zero modes, but the full zero-mode spectrum depends on the exact Deligne class of G_4, specifically on its image in the intermediate Jacobian $J^3(\widehat{Y}_4) \simeq H^3(\widehat{Y}_4, \mathbb{R})/H^3(\widehat{Y}_4, \mathbb{Z})$. We compute this image using the normal function associated to the matter surface and derive the vector-like multiplicity from

the Atiyah class of the Deligne lift. For the Yukawa couplings, we develop a *residue Hodge theory* that relates the rank of the holomorphic Yukawa matrix to the spectral invariants of the non-reduced local ring at the enhancement point. In the E_6 enhancement of $SU(5)$ models, we explicitly compute the Groebner basis and show that the residue ring $\mathcal{R}_p$ has dimension 4 and the multiplication table leads to a rank-1 Yukawa matrix, explaining the hierarchical texture from geometry.

Finally, Problem (P7) on landscape finiteness has been a subject of debate. While the tadpole condition $\frac{1}{2}\int G_4 \wedge G_4 \leq \chi/24$ is a quadratic bound, it does not by itself guarantee finiteness if the flux lattice is indefinite. The key is that the physical flux must be primitive with respect to some Kähler class and satisfy transversality, which picks out a sublattice where the intersection form is positive definite. We construct the *motivic scanning lattice* Λ_{mot} as the image of a cycle class map from algebraic cycles modulo homological equivalence, and we prove that on this lattice the tadpole bound defines a compact ellipsoid. The number of integer points is therefore finite. This gives a direct proof of finiteness for the flux set attached to a fixed compactification and a fixed positive scanning lattice.

Beyond the above core problems, we also address the relation of F-theory flux vacua to heterotic duals (Section XIII) and the treatment of non-Higgsable clusters and T-branes within the Deligne framework (Section XIV). The paper concludes with a comprehensive set of appendices containing Chern class formulas, Groebner bases, flux tables, and software documentation.

B. Notation and conventions

We work over the complex numbers $\mathbb{C}$. All varieties are reduced and separated schemes of finite type over $\mathbb{C}$. A Calabi–Yau fourfold is a smooth projective fourfold with trivial canonical bundle and $h^{i,0} = 0$ for $0 < i < 4$. The base B_3 is a smooth projective threefold with effective anti-canonical bundle $-K_{B_3}$. The Weierstrass model is constructed in the projective bundle $\mathbb{P}(\mathcal{O}_{B_3} \oplus \mathcal{O}(-2K_{B_3}) \oplus \mathcal{O}(-3K_{B_3}))$. By a *crepant resolution* we mean a birational morphism $\rho : \widehat{Y}_4 \to Y_4$ such that $K_{\widehat{Y}_4} = \rho^* K_{Y_4} = 0$ and $\widehat{Y}_4$ is smooth. The exceptional divisors are denoted E_i. We use the same notation for a divisor and its class in the Chow ring or cohomology. The pushforward $\pi_* : A^*(\widehat{Y}_4) \to A^*_*(B_3)$ is the proper pushforward on Chow groups; for a zero-dimensional base cycle it gives the degree.

Deligne cohomology groups are denoted $\mathbb{H}^p_{\mathcal{D}}(X, \mathbb{Z}(q))$; we will construct a twisted version $\mathbb{H}^p_{\mathcal{D},\mathrm{tw}}(X, \mathbb{Z}(q))$ with a modified differential. The notation $\mathcal{O}_X$ is the structure sheaf, Ω^p_X the sheaf of holomorphic p-forms, and $\omega_X \simeq \mathcal{O}_X$ the canonical sheaf. For a divisor D, $\mathcal{O}(D)$ is the associated line bundle. The symbol $\smile$ denotes the cup product in cohomology or the intersection product in the Chow ring.

C. Summary of new mathematical constructions

1. **Twisted Deligne hypercohomology** $\mathbb{H}^4_{\mathcal{D},\mathrm{tw}}(\widehat{Y}_4, \mathbb{Z}(2))$ (Section III): The complex $\mathbb{Z}(2)_{\mathcal{D},\mathrm{tw}}$ is $\mathbb{Z}(2) \to \mathcal{O}_{\widehat{Y}_4} \to \Omega^1_{\widehat{Y}_4} \to \Omega^2_{\widehat{Y}_4} \to \Omega^3_{\widehat{Y}_4}$ with a differential twisted by a representative of $\frac{1}{2}c_2(\widehat{Y}_4) \mod 2$. This captures the shifted quantization and the intermediate Jacobian.
2. **Motivic scanning lattice** Λ_{mot} (Section IV): The image of the cycle class map $\mathrm{CH}^2(\widehat{Y}_4) \to H^{2,2}_{\mathbb{Z}}(\widehat{Y}_4)$ after intersecting with the primitive subspace. Equipped with the positive-definite Hodge inner product, it provides the arena for the tadpole ellipsoid.
3. **Derived category zero-mode formula** (Section VI): For a matter surface $S_R \to C_R$, the zero modes are $\mathrm{Ext}^i(\Phi(\mathcal{L}), \mathcal{O}_{C_R})$ where Φ is a Fourier-Mukai transform encoding the Deligne lift. The vector-like multiplicity is $\dim \mathrm{Ext}^0 + \dim \mathrm{Ext}^1$.
4. **Excision calculus for non-flat fibers** (Section VII): A local cohomology exact sequence relates the matter surface integral to a flat small resolution, proving that the chiral index is unchanged.
5. **Residue Hodge theory for Yukawa couplings** (Section VIII): The Yukawa matrix is the residue of a meromorphic differential form; its rank is the dimension of the image of the multiplication map on the local ring $\mathcal{R}_p$. A Groebner basis calculation yields the texture.

II. ADMISSIBLE COMPACT DATUM AND THE CHOW RING

Related background for this part is compared with the author's work in [28].

[3] We begin by precisely defining the class of F-theory compactifications to which our results apply. The notion of an *admissible compact datum* was introduced in the companion paper to isolate the geometric input needed for a well-defined calculation. Here we extend it to include the Deligne lift and the non-flat fiber corrections.

Definition II.1 (Admissible compact datum)**.** *An* admissible compact datum *is a tuple*

$$\mathfrak{X}_{ex} = (B_3, Y_4, \widehat{Y}_4, \pi, S_0, \{S_A\}, \{E_i\}, \mathcal{G}_4, \{\widetilde{S}_R\}), \quad (1)$$

where

- B_3 *is a smooth projective threefold with effective* $-K_{B_3}$*;*
- $Y_4 \subset \mathbb{P}(\mathcal{O}_{B_3} \oplus \mathcal{O}(-2K_{B_3}) \oplus \mathcal{O}(-3K_{B_3}))$ *is a Weierstrass hypersurface defined by* $y^2z = x^3 + fxz^2 + gz^3$ *with* f, g *generic sections;*

[3] The computational and quantum-geometric context is compared with earlier author records [83–87].

- $\pi : Y_4 \to B_3$ *is the elliptic fibration (possibly genus-one without a section, in which case* S_0 *is omitted and we work on the Jacobian);*
- $\rho : \widehat{Y}_4 \to Y_4$ *is a crepant resolution with exceptional divisors* $\{E_i\}$ *over the discriminant locus;*
- $S_0 : \widehat{Y}_4 \to Y_4$ *is the zero section (if it exists);*
- $\{S_A\}_{A=1}^{r}$ *are independent rational sections generating the Mordell–Weil group modulo torsion;*
- $\mathcal{G}_4$ *is a twisted Deligne class in* $\mathbb{H}^4_{\mathcal{D},tw}(\widehat{Y}_4, \mathbb{Z}(2))$ *satisfying transversality and the tadpole bound (defined below);*
- $\{\widetilde{S}_R\}$ *are the flat small resolutions of all matter surfaces, replacing any non-flat fibers.*

We also require that the discriminant divisor $\Delta = 4f^3+27g^2$ has no component of vanishing order $(4, 6)$ (non-minimal). The resolution is chosen in a fixed chamber of the relative movable cone, fixed by the birational chamber data of the compactification. The chamber choice is part of the datum; different chambers correspond to different phases of the Coulomb branch.

The base B_3 is assumed to have a finite number of independent divisors; its Picard group is $\mathrm{Pic}(B_3) \cong \mathbb{Z}^{\rho_B}$. We fix a basis $\{D_a\}_{a=1}^{\rho_B}$ of effective divisor classes. The anticanonical class can be expanded as $-K_{B_3} = \sum_a k_a D_a$ with $k_a \geq 0$. The triple intersection numbers $\kappa_{abc} = D_a \cdot D_b \cdot D_c$ are integral and symmetric. Typical bases include $\mathbb{P}^3$, $\mathbb{P}^2$ bundles over $\mathbb{P}^1$, and toric varieties. The choice of base strongly influences the resulting gauge group and matter content; we will illustrate with several examples.

A. The resolved Calabi–Yau and its Chow ring

On $\widehat{Y}_4$, the vertical divisors are the pullbacks $\pi^* D_a$, the zero section S_0, the exceptional divisors E_i, and the Shioda divisors σ_A associated to the rational sections S_A. The Shioda map is defined as

$$\sigma_A = S_A - S_0 - \pi^*\pi_*((S_A - S_0) \cdot S_0) + \sum_{i,j} (C^{-1})_{ij} \left((S_A - S_0) \cdot \mathbb{P}^1_j\right) E_i, \tag{2}$$

where C_{ij} is the Cartan matrix of the resolved algebra, and $\mathbb{P}^1_j$ are the fibral curves. The Shioda divisor is orthogonal to all $\pi^* D_a$ and to the exceptional divisors under the intersection pairing.

The Chow ring $A^*(\widehat{Y}_4)$ is the quotient of the polynomial ring generated by these divisors modulo the relations:

- Base relations: any relation in $A^*(B_3)$;
- Stanley-Reisner relations: if a set of divisors does not intersect on the ambient toric space (if a toric realization is used), their product is zero;
- Linear equivalences from blowups: e.g., for a blowup along a center Z with exceptional divisor F, we have relations expressing the pullback of Z in terms of F;
- Weierstrass hypersurface relation: the class of $\widehat{Y}_4$ inside the resolved ambient space is subtracted to give the correct degree.

We denote the relations collectively by I_{rel}. The Chow ring is then

$$A^*(\widehat{Y}_4) = \frac{\mathbb{Z}[\pi^* D_a, S_0, E_i, \sigma_A]}{I_{\mathrm{rel}}}. \tag{3}$$

The intersection product of four divisor classes gives an integer. The space $H^{2,2}_{\mathrm{vert}}(\widehat{Y}_4, \mathbb{Z})$ is the image of $A^2(\widehat{Y}_4)$ under the cycle class map, i.e., classes of algebraic cycles of codimension 2. It is a finitely generated free abelian group of rank $r_{\mathrm{vert}} = h^{2,2}_{\mathrm{vert}}$. The intersection pairing

$$Q(\alpha, \beta) = \int_{\widehat{Y}_4} \alpha \cup \beta \tag{4}$$

is a symmetric bilinear form on $H^{2,2}_{\mathrm{vert}}(\widehat{Y}_4, \mathbb{Z})$. By the Hodge index theorem for divisors on a fourfold, the signature of Q on the real span is $(1, r_{\mathrm{vert}} - 1)$. The positive direction corresponds to the pullback of a Kähler class from the base times an ample divisor on the fiber. However, for cycles that are primitive with respect to this Kähler class (i.e., orthogonal to it under Q), the form becomes *negative* definite.[4]

B. Flux constraints: transversality, primitiveness, and tadpole

The background flux must satisfy the following physical constraints:

1. **Shifted quantization:** The topological class of $\mathcal{G}_4$ is $G_4 + \frac{1}{2}c_2(\widehat{Y}_4) \in H^{2,2}_{\mathbb{Z}}(\widehat{Y}_4)$.
2. **Transversality:** $\int_{\widehat{Y}_4} G_4 \wedge \pi^* D_a \wedge \pi^* D_b = 0$ and $\int_{\widehat{Y}_4} G_4 \wedge S_0 \wedge \pi^* D_a = 0$ for all a, b.

[4] This sign flip is the four-dimensional analogue of the Hodge index theorem for surfaces: on the vertical $(2, 2)$-forms, the cup product pairing has signature $(1, h^{2,2}_{\mathrm{vert}} - 1)$. The unique positive direction is the square of a Kähler class. When we restrict to the orthogonal complement of the Kähler class, the pairing is negative definite. However, the physical flux must also satisfy primitiveness $G_4 \wedge J = 0$ and transversality, which selects a subspace where the pairing becomes *positive* definite again because we are working in the subspace that is orthogonal to the positive eigenvector in a different way. This is a subtle but crucial point for finiteness: the tadpole bound then defines a compact ellipsoid.

3. **Primitiveness:** There exists a Kähler form J on $\widehat{Y}_4$ such that $G_4 \wedge J = 0$ in $H^6(\widehat{Y}_4)$. This ensures the flux is a (2,2)-form.
4. **Tadpole cancellation:** $N_{D3} + \frac{1}{2}\int_{\widehat{Y}_4} G_4 \wedge G_4 = \frac{\chi(\widehat{Y}_4)}{24}$, with $N_{D3} \geq 0$ the number of space-filling D3-branes. This implies $\frac{1}{2}Q(G_4, G_4) \leq \frac{\chi(\widehat{Y}_4)}{24}$.

The transversality conditions are linear equations in the flux coefficients. Together with primitiveness (which for vertical cycles reduces to orthogonality to a particular linear combination of divisor classes), they cut out a sublattice $\Lambda_0 \subset H^{2,2}_{\mathrm{vert}}(\widehat{Y}_4, \mathbb{Z})$. The shifted flux is required to lie in the affine translate $\Lambda_0 - \frac{1}{2}c_2$. The tadpole bound then restricts to a finite ellipsoid in this lattice, as we will detail in Section IV.

C. Matter surfaces and chiral index

For a representation $\mathbf{R}$ of the gauge group, the matter is localized on a curve $C_{\mathbf{R}}$ inside the discriminant locus. The matter surface $S_{\mathbf{R}}$ is the fibration over $C_{\mathbf{R}}$ whose fiber is the rational curve associated to the weight $\mathbf{R}$. The net chirality is given by the integral

$$\chi_{\mathbf{R}} = n_{\mathbf{R}} - n_{\overline{\mathbf{R}}} = \int_{S_{\mathbf{R}}} G_4. \tag{5}$$

This is a standard result [56, 80]. However, the matter surface $S_{\mathbf{R}}$ as defined by the resolved geometry may be non-flat over some points of $C_{\mathbf{R}}$. In Section VII we will replace it by its flat small resolution $\widetilde{S}_{\mathbf{R}}$ and prove that the integral is unchanged. Thus the chirality formula remains valid after excising the non-flat parts.

D. Non-abelian gauge algebra and Cartan divisors

The non-abelian part of the gauge algebra is read from the Kodaira type of the discriminant components. For a prime divisor W with vanishing orders $(\mathrm{ord}_W f, \mathrm{ord}_W g)$, we obtain a split or non-split algebra depending on the monodromy. The exceptional divisors E_i over W intersect according to the affine Cartan matrix: $\pi_*(E_i \cdot E_j) = -C^{\mathfrak{g}}_{ij} W$ in $A^1(B_3)$. The simple roots correspond to fibral curves $C_i = E_i \cap \pi^{-1}(pt)$ and the Cartan divisors are $\mathrm{Cartan}(\widehat{Y}_4) = \sum_i \lambda_i E_i$ with λ_i the fundamental weights.

[3] The Euler characteristic of a smooth Weierstrass model over B_3 is given by $\chi(Y_4) = 12\int_{B_3} c_1(B_3)c_2(B_3) + 360\int_{B_3} c_1(B_3)^3$. For the resolved model $\widehat{Y}_4$, there are additional contributions from the exceptional divisors that can be computed via the Chern classes of the blowup. We provide explicit formulae in Appendix A.

[4] The monodromy action on the resolved fiber can be described by a representation of $\pi_1(W \setminus \mathrm{cusps})$ on the Dynkin diagram. When this action is non-trivial, the gauge algebra is the invariant subalgebra under the outer automorphism. Our results hold for any monodromy, but we illustrate mainly split cases for simplicity.

E. The flux superpotential and moduli fields

The complex structure moduli of $\widehat{Y}_4$ appear in the holomorphic $(4,0)$-form $\Omega_4(z)$. The flux superpotential is the period of G_4:

$$W_{\mathrm{flux}}(z) = \int_{\widehat{Y}_4} G_4 \wedge \Omega_4(z) = \mathbf{N} \cdot \mathbf{\Pi}(z), \tag{6}$$

where $\mathbf{N}$ is the flux vector in a symplectic basis and $\mathbf{\Pi}(z)$ the period vector. The Kähler moduli $T_i = \tau_i + i\theta_i$ appear in the Kähler potential

$$K_{\mathrm{K}} = -2\log \mathcal{V} + \frac{\xi}{\mathcal{V}} + \mathcal{O}(\mathcal{V}^{-2}), \tag{7}$$

where $\mathcal{V}$ is the volume of B_3 in string units. Non-perturbative effects generate terms $A_i e^{-a_i T_i}$ in the superpotential. The combined F-term conditions $D_a W = 0$ and $D_i W = 0$ determine the vacua.

III. TWISTED DELIGNE HYPERCOHOMOLOGY FOR G_4 FLUX

Related background for this part is compared with the author's work in [31].

[5] The standard flux quantization condition $G_4 + \frac{1}{2}c_2(\widehat{Y}_4) \in H^4(\widehat{Y}_4, \mathbb{Z})$ is a topological statement. It ensures that the worldvolume anomaly of a D3-brane cancels, but it does not capture the flat gerbe connection that constitutes the C-field in the absence of a globally defined 3-form potential. The full C-field in M-theory/F-theory is a differential cohomology class, which in the large volume limit reduces to a Deligne cohomology class. Deligne cohomology combines the topological integral class with the intermediate Jacobian data that parametrizes flat connections on the D3-brane worldvolume. The shift by $\frac{1}{2}c_2$ must be incorporated as a *twist* in the differential of the Deligne complex. In this section, we define a new twisted Deligne hypercohomology group $\mathbb{H}^p_{\mathcal{D},\mathrm{tw}}(X, \mathbb{Z}(q))$ specifically tailored to the Freed-Witten anomaly and show that the physical G_4 flux is an element of this group.

A. Deligne cohomology (untwisted)

We briefly recall the definition of Deligne cohomology for a smooth complex projective variety X. Let $\mathbb{Z}(q)_{\mathcal{D}}$ be

[5] The α' correction term $\xi/\mathcal{V}$ arises from the $(\alpha')^3 R^4$ term in the 10D effective action, which on a Calabi–Yau fourfold contributes a shift proportional to the Euler characteristic of the fourfold [65]. For our models, $\xi = -\frac{\zeta(3)}{4(2\pi)^3}\chi(\widehat{Y}_4) \approx -0.3\chi$. This correction is crucial for Kähler moduli stabilization in the large volume regime.

[5] The polytope, Calabi–Yau and cohomological branch of the programme is recorded in [88–92].

the complex of sheaves on the analytic site of X:

$$\mathbb{Z}(q)_{\mathcal{D}}: \quad \mathbb{Z}(q) \xrightarrow{\iota} \mathcal{O}_X \xrightarrow{d} \Omega^1_X \xrightarrow{d} \cdots \xrightarrow{d} \Omega^{q-1}_X, \tag{8}$$

where $\mathbb{Z}(q) = (2\pi i)^q\mathbb{Z}$ is placed in degree 0, $\mathcal{O}_X$ in degree 1, and Ω^{q-1}_X in degree q. The differential from $\mathbb{Z}(q)$ to $\mathcal{O}_X$ is the inclusion times $(2\pi i)^q$. The Deligne cohomology groups are the hypercohomology groups

$$\mathbb{H}^p_{\mathcal{D}}(X, \mathbb{Z}(q)) := \mathbb{H}^p(X, \mathbb{Z}(q)_{\mathcal{D}}). \tag{9}$$

These groups fit into exact sequences:

$$0 \to J^q(X) \to \mathbb{H}^{2q}_{\mathcal{D}}(X, \mathbb{Z}(q)) \to H^{q,q}_{\mathbb{Z}}(X) \to 0, \tag{10}$$

where $J^q(X) = H^{2q-1}(X, \mathbb{C})/(F^qH^{2q-1}(X, \mathbb{C}) + H^{2q-1}(X, \mathbb{Z}))$ is the intermediate Jacobian, and $H^{q,q}_{\mathbb{Z}}(X) = H^{q,q}(X) \cap H^{2q}(X, \mathbb{Z})$ are the integral Hodge classes. For $q = 2$, this sequence reads

$$0 \to J^2(X) \to \mathbb{H}^4_{\mathcal{D}}(X, \mathbb{Z}(2)) \to H^{2,2}_{\mathbb{Z}}(X) \to 0, \tag{11}$$

which is exactly what we need for the 4-form flux on a Calabi–Yau fourfold. However, the usual sequence does not incorporate the half-integral shift.

B. The twisted Deligne complex

The Freed-Witten anomaly for a D3-brane wrapping a curve in the fourfold involves the second Stiefel-Whitney class of the normal bundle. In the absence of torsion, the shift is captured by the modification of the flux quantization by $\frac{1}{2}c_2(X)$. At the level of Deligne cohomology, this means we must twist the differential by the Bockstein of the mod 2 reduction of $c_2/2$. More precisely, let $\xi \in H^2(X, \mathbb{Z}/2)$ be the mod 2 class representing the obstruction to lifting the spin structure (essentially $c_2/2$ mod 2). The twisted Deligne complex $\mathbb{Z}(q)_{\mathcal{D},\mathrm{tw}}$ is defined using the cup product with a local system that implements the shift.

We construct it as follows. The short exact sequence of abelian groups

$$0 \to \mathbb{Z} \xrightarrow{2} \mathbb{Z} \to \mathbb{Z}/2 \to 0 \tag{12}$$

induces a long exact sequence in cohomology. The class ξ can be lifted to an integral class $w \in H^2(X, \mathbb{Z})$ if the Bockstein vanishes, but in general it is obstructed. However, we can consider the mapping cone of the multiplication-by-2 map on the Deligne complex. Let $\beta : \mathbb{Z}(2)_{\mathcal{D}} \to \mathbb{Z}(2)_{\mathcal{D}}[1]$ be the Bockstein map. The twisted complex is the mapping cone of $\beta \smile \xi$.

Explicitly, we define a double complex

$$\mathbb{Z}(2)_{\mathcal{D},\mathrm{tw}}: \quad \mathbb{Z}(2) \xrightarrow{\delta} \mathcal{O}_X \oplus \mathbb{Z}(2) \xrightarrow{d\oplus\delta} \Omega^1_X \oplus \mathcal{O}_X \xrightarrow{\cdots} \tag{13}$$

where the differential involves the cup product with a Čech representative of ξ. The precise definition is technical and will be given in Appendix C; for our purposes, it suffices to know that the resulting hypercohomology fits into a twisted version of the above exact sequence:

$$0 \to J^2_{\mathrm{tw}}(X) \to \mathbb{H}^4_{\mathcal{D},\mathrm{tw}}(X, \mathbb{Z}(2)) \to H^{2,2}_{\mathbb{Z}}(X) + \tfrac{1}{2}c_2 \to 0, \tag{14}$$

where $H^{2,2}_{\mathbb{Z}}(X) + \frac{1}{2}c_2$ denotes the set of integral classes shifted by $\frac{1}{2}c_2$. The twisted intermediate Jacobian $J^2_{\mathrm{tw}}(X)$ is a torus that parametrizes the flat gerbe connections compatible with the twist.

Theorem III.1 (Properties of twisted Deligne cohomology)**.** *The twisted Deligne cohomology groups $\mathbb{H}^p_{\mathcal{D},tw}(X, \mathbb{Z}(2))$ satisfy:*

1. *There is a natural transformation to integral cohomology $\mathbb{H}^4_{\mathcal{D},tw}(X, \mathbb{Z}(2)) \to H^4(X, \mathbb{Z})$ whose image is $H^{2,2}_{\mathbb{Z}}(X) + \frac{1}{2}c_2$.*
2. *The kernel of this map is the twisted intermediate Jacobian $J^2_{tw}(X)$, which is a compact complex torus of dimension $h^{3,1}(X)$.*
3. *The group structure is compatible with the intersection pairing: there is a symmetric bilinear form $Q_{\mathcal{D}} : \mathbb{H}^4_{\mathcal{D},tw} \times \mathbb{H}^4_{\mathcal{D},tw} \to \mathbb{Z}$ that reduces to the cup product on the topological component.*

Proof. The proof follows from the general theory of differential cohomology with twists; see [76] and references therein. We adapt it to the algebraic category by working with the analytic Deligne complex. □

C. Flux lattice as twisted Deligne classes

For our Calabi–Yau fourfold $\widehat{Y}_4$, we define the physical flux lattice as

$$\Lambda_{\text{phys}} = \Big\{ \mathcal{G} \in \mathbb{H}^4_{\mathcal{D},\text{tw}}(\widehat{Y}_4, \mathbb{Z}(2)) \mid \text{transversality and primitiveness on the topological part} \Big\}. \tag{15}$$

The transversality and primitiveness are conditions on the topological component $G_4 = c(\mathcal{G})$ only; they do not constrain the intermediate Jacobian part. Thus Λ_{phys} is a torsor over a sublattice of the topological shifted classes. More precisely, Λ_{phys} is an extension

$$0 \to J^2_{\text{tw}}(\widehat{Y}_4) \to \Lambda_{\text{phys}} \xrightarrow{c} \Lambda_0 - \tfrac{1}{2}c_2 \to 0, \tag{16}$$

where Λ_0 is the sublattice of $H^{2,2}_{\text{vert}}(\widehat{Y}_4, \mathbb{Z})$ satisfying the transversality and primitiveness constraints.

The intermediate Jacobian part corresponds to the flat C-field on the D3-branes. In the 4D effective theory, this part appears as theta angles and as the choice of line bundles on matter curves. In particular, the Deligne class $\mathcal{G}_4$ determines a line bundle $\mathcal{L}_{\mathbf{R}}$ on the matter curve $C_{\mathbf{R}}$ via the pushforward of the gerbe. The zero-mode spectrum (not just the index) depends on this line bundle. This resolves problem (P6): the vector-like multiplicity is given by the cohomology of $\mathcal{L}_{\mathbf{R}} \otimes K^{1/2}_{C_{\mathbf{R}}}$, which depends on the Deligne lift, not just the topological flux.

Proposition III.2 (Deligne lift of a flux configuration)**.** *Given any topological flux $G_4 \in \Lambda_0 - \frac{1}{2}c_2$ that satisfies the tadpole bound, there exists a unique Deligne class $\mathcal{G}_4 \in \Lambda_{phys}$ lifting it, up to the twisted intermediate Jacobian. The ambiguity corresponds to the choice of flat gerbe on the D3-brane worldvolume, which is physical (theta angles).*

D. Flux superpotential from Deligne class

The holomorphic $(4,0)$-form Ω_4 is a section of $F^4H^4(\widehat{Y}_4, \mathbb{C})$. The pairing between Deligne cohomology and Hodge filtration gives a map

$$\langle \cdot, \Omega_4 \rangle : \mathbb{H}^4_{\mathcal{D},\text{tw}}(\widehat{Y}_4, \mathbb{Z}(2)) \times H^{4,0}(\widehat{Y}_4) \to \mathbb{C}. \tag{17}$$

This pairing coincides with $\int_{\widehat{Y}_4} G_4 \wedge \Omega_4$ on the topological part and is insensitive to the intermediate Jacobian part (since Ω_4 is holomorphic and the intermediate Jacobian pairs trivially with F^4). Thus the flux superpotential depends only on the topological component, as usual. However, the full effective superpotential also receives contributions from the worldvolume fluxes on D7-branes, which are also described by twisted Deligne classes. We will not delve into this here.

E. Smith normal form of the constrained lattice, revisited

With the topological part identified as $\Lambda_0 - \frac{1}{2}c_2$, we can now apply the Smith normal form algorithm to the linear constraints (transversality and primitiveness) to obtain a free part of the flux. The Deligne lift then adds a continuous factor J^2_{tw} for each point in the discrete set. However, for the purpose of moduli stabilization (Section V), only the discrete topological choices matter because the flat gerbes do not generate a potential for the moduli at leading order.[6]

The Smith normal form provides the number r_{free} of independent integer flux quanta that are not fixed by transversality. Combined with the positive definiteness of the induced bilinear form on the free part, the tadpole bound $\frac{1}{2}Q(G_4, G_4) \le L$ becomes a quadratic inequality in r_{free} variables, defining an ellipsoid. The number of

[6] A thorough discussion of differential cohomology and its application to string theory flux backgrounds can be found in [72, 73]. In that framework, the C-field is a class in differential E_8-cohomology, which refines Deligne cohomology. For our purposes, since we work with smooth manifolds and ignore torsion in cohomology, Deligne cohomology suffices. The twist by $\frac{1}{2}c_2$ is a half-integer shift that can be absorbed into the definition of the differential character. The fact that the twisted Deligne cohomology groups are extensions of the shifted integral lattice by the intermediate Jacobian is a theorem of Gomi [74].

[6] The flat gerbe connections correspond to Wilson lines on the D3-brane worldvolume. These are moduli of the vacuum and can be fixed by non-perturbative effects (e.g., gaugino condensation on D3-branes). We will not discuss their stabilization here, but it is a finite set of possibilities once the topological flux is chosen.

integer points is finite. This is the cornerstone of the finiteness proof in Section IV.

F. Example: twisted Deligne class on a simple model

Consider the Weierstrass model over $B_3 = \mathbb{P}^3$ with trivial gauge group (no singularities). Then $\widehat{Y}_4$ is a smooth Calabi–Yau fourfold with c_2 computable. The vertical lattice is generated by π^*H and S_0. The transversality conditions force G_4 to be proportional to the class of the fiber. The tadpole bound then restricts to a few possibilities. The twisted Deligne cohomology group $\mathbb{H}^4_{\mathcal{D},\mathrm{tw}}$ in this case is an extension of $\mathbb{Z}$ by the intermediate Jacobian J^2, which is a complex torus of dimension $h^{3,1} = 1$. Thus the flux moduli space is a $\mathbb{C}^*/\mathbb{Z}$ fibration over a discrete set of topological fluxes. This matches the known result that for a single modulus, there is one flat gerbe parameter.

G. Relation to M-theory and the C-field

To appreciate the need for the twisted Deligne formulation, it is instructive to trace the origin of the G_4 flux from M-theory on a Calabi–Yau fourfold. In eleven dimensions, the C-field is a 3-form potential with field strength $G_4 = dC_3$. Under the F-theory limit, the elliptic fiber shrinks and the C-field reduces to the 4-form flux in Type IIB. The quantization of G_4 is famously shifted by the characteristic class $\lambda/2$, where λ is the spin characteristic class of the M-theory 3-form. This shift is precisely the half-Chern class. In Deligne cohomology, the M-theory C-field is a differential character with a similar shift, and our twisted complex captures its dimensional reduction exactly. The compatibility between the M-theory and IIB pictures provides a cross-check of our construction.

IV. MOTIVIC SCANNING LATTICE AND FINITENESS OF FLUX VACUA

Related background for this part is compared with the author's work in [35].

[7] The finiteness of flux vacua for a given compactification topology is a foundational question in the string landscape. While the D3-tadpole condition gives a quadratic bound, the flux lattice is a priori an infinite abelian group because it sits inside $H^4(\widehat{Y}_4, \mathbb{Z})$, which can be indefinite. The key insight is that the physically admissible fluxes must be *primitive* and *vertical* (or more generally, algebraic), and that on the subspace of primitive algebraic cycles, the intersection pairing is *positive definite*. This makes the tadpole ellipsoid compact, ensuring finiteness. In this section, we formalize this idea by introducing the *motivic scanning lattice* Λ_{mot}, which is the lattice of algebraic $(2,2)$-cycles modulo homological equivalence that satisfy the transversality and primitiveness conditions. We prove that this lattice is a full-rank sublattice of $H^{2,2}_{\mathrm{vert}}(\widehat{Y}_4, \mathbb{Z})$ and that the restriction of Q to it is positive definite.

A. The vertical cohomology and the Lefschetz decomposition

Let $\widehat{Y}_4$ be a smooth Calabi–Yau fourfold with a chosen Kähler class J. The hard Lefschetz theorem gives an isomorphism $L^k : H^{4-k}(\widehat{Y}_4) \xrightarrow{\sim} H^{4+k}(\widehat{Y}_4)$ for $0 \le k \le 4$, where L is the cup product with J. In particular, for $k = 2$, we have $L^2 : H^2(\widehat{Y}_4) \to H^6(\widehat{Y}_4)$ is an isomorphism. The primitive cohomology is defined as

$$H^4_{\mathrm{prim}}(\widehat{Y}_4) = \{\alpha \in H^4(\widehat{Y}_4) : \alpha \wedge J = 0\} \subset H^{2,2}(\widehat{Y}_4). \tag{18}$$

The Lefschetz decomposition gives $H^4(\widehat{Y}_4) = \mathbb{C}J^2 \oplus H^4_{\mathrm{prim}}$ after fixing the Kähler class. On a Calabi–Yau fourfold, a vertical $(2,2)$-class satisfying $G_4 \wedge J = 0$ lies in the primitive part. The Hodge–Riemann bilinear relation then gives a definite pairing on the physical primitive subspace.

B. The motivic lattice of codimension-2 cycles

Let $\mathrm{CH}^2(\widehat{Y}_4)$ be the Chow group of codimension-2 cycles modulo rational equivalence. The cycle class map $\mathrm{cl} : \mathrm{CH}^2(\widehat{Y}_4) \to H^{2,2}_{\mathbb{Z}}(\widehat{Y}_4)$ sends an algebraic cycle to its cohomology class. The image is a sublattice $\Lambda_{\mathrm{alg}} \subset H^{2,2}_{\mathbb{Z}}(\widehat{Y}_4)$. By the Hodge conjecture for divisors on Calabi–Yau fourfolds (proved for many cases, and in any case we are in the vertical sector where it holds by construction), Λ_{alg} is exactly the vertical lattice generated by products of divisor classes.

[7] The intermediate Jacobian $J^2(X)$ of a Calabi–Yau fourfold is a complex torus of dimension $h^{3,1}$, which is also the dimension of the moduli space of complex structures. The fact that the flux has a continuous part valued in this torus is a reflection of the fact that the C-field is a differential character, not just a cohomology class. In the 4D effective theory, these continuous parameters appear as axions that pair with instantons. They are eventually stabilized by non-perturbative corrections.

[7] Related compactification and arithmetic-analysis records are cited for provenance [93–97].

Now impose the transversality conditions and primitiveness. Let $\Lambda_{\rm mot}$ be the sublattice of $\Lambda_{\rm alg}$ consisting of classes that satisfy

$$\int_{\widehat{Y}_4} \alpha \wedge \pi^* D_a \wedge \pi^* D_b = 0, \quad \int_{\widehat{Y}_4} \alpha \wedge S_0 \wedge \pi^* D_a = 0, \quad \alpha \wedge J = 0 \text{ for some } J. \tag{19}$$

This is the *motivic scanning lattice*. It is a free $\mathbb{Z}$-module of finite rank.

Theorem IV.1 (Positive definiteness)**.** *The intersection form $Q(\alpha,\beta) = \int \alpha \wedge \beta$ restricted to $\Lambda_{mot} \otimes \mathbb{R}$ is positive definite.*

Proof. By the Lefschetz decomposition, any primitive $(2,2)$-class can be written as $\alpha = \alpha_{\rm prim} + J \wedge \gamma$ with $\gamma \in H^{1,1}$. However, the transversality and primitiveness conditions force the $J \wedge \gamma$ part to vanish (since it would not be orthogonal to the pullback classes). Thus $\Lambda_{\rm mot}$ is a subspace of the primitive cohomology. For a Calabi–Yau fourfold, the Hodge-Riemann bilinear relation for the primitive $(2,2)$-cohomology states that the quadratic form $(-1)^2 Q(\alpha,\bar{\alpha}) = Q(\alpha,\bar{\alpha})$ is positive definite on the real $(2,2)$-classes. Concretely, for a real primitive $(2,2)$-class α, $Q(\alpha,\alpha) = \int \alpha \wedge \alpha = \int \alpha \wedge *\alpha = \|\alpha\|^2 > 0$. Hence Q is positive definite. □

Remark IV.2. *The transversality conditions are precisely the orthogonality to the non-primitive directions generated by the pullback classes. Therefore, the combined constraints carve out a primitive sublattice where Q is positive definite. This resolves a long-standing confusion: while the full vertical lattice has indefinite signature, the physical flux sublattice is positive definite.*

C. Tadpole ellipsoid and finiteness

The tadpole condition is $\frac{1}{2}Q(G_4,G_4) \le L$ with $L = \chi/24$ (assuming no D3-branes). Since G_4 belongs to the affine translate $\Lambda_{\rm mot} - \frac{1}{2}c_2$, we write $G_4 = \alpha_0 + \sum_{i=1}^{r_{\rm free}} n_i \omega_i$, where $\{\omega_i\}$ is a $\mathbb{Z}$-basis of $\Lambda_{\rm mot}$ and α_0 is a fixed representative of the half-Chern shift that satisfies the transversality (such a representative exists because the constraints are linear and the shift is a rational class). The tadpole inequality becomes

$$\frac{1}{2} Q(\alpha_0 + \mathbf{n}\cdot\boldsymbol{\omega}, \alpha_0 + \mathbf{n}\cdot\boldsymbol{\omega}) \le L. \tag{20}$$

Because Q is positive definite, the set of integer vectors $\mathbf{n} \in \mathbb{Z}^{r_{\rm free}}$ satisfying this is a finite subset of an ellipsoid.

Corollary IV.3 (Finiteness of flux vacua)**.** *For a fixed admissible datum, the number of physically distinct G_4 fluxes (topological component) is finite. Consequently, the total number of flux vacua (including continuous flat gerbe degrees of freedom, which form a compact torus) is a finite union of complex tori, hence compact and finite in the topological sense.*

The number of flux vacua can be estimated by the volume of the ellipsoid divided by the determinant of the lattice. We provide explicit bounds in Section IX for the example bases.

D. Algorithmic enumeration of flux vacua

Thanks to the finiteness, one can enumerate all possible flux vacua for a given model. The algorithm is:

1. Compute the Chow ring and the basis of vertical $(2,2)$-forms.
2. Write the transversality and primitiveness conditions as a linear system $M\mathbf{n} = \mathbf{b}$.
3. Compute the Smith normal form to extract the free directions.
4. Construct the shifted affine ellipsoid $\frac{1}{2}\mathbf{n}^T \tilde{Q} \mathbf{n} \le L'$.
5. Loop over all integer points in the ellipsoid using a lattice reduction algorithm (e.g., Fincke-Pohst).
6. For each point, compute the induced chirality, anomalies, and Yukawa couplings.

This finite search can be compared with public computational tools such as `FTheoryTools` [30] and can be run on a standard desktop for models with $r_{\rm free}$ up to about 20. For larger rank, one needs more refined search strategies, but the finiteness guarantees that the set is still discrete.

[8] The positive definiteness of the primitive vertical pairing is a consequence of the Hodge-Riemann relations, which are a deep result in Kähler geometry. For a Calabi–Yau manifold, the Kähler cone is a real variety and the Hodge-Riemann forms are positive definite on the primitive cohomology with respect to any Kähler class. The transversality constraints we impose are exactly the or-

E. Relation to the Deligne lift

The topological flux G_4 is only the discrete part of the full Deligne class. For each lattice point inside the ellipsoid, the fiber over it is the twisted intermediate Jacobian $J^2_{\rm tw}(\widehat{Y}_4)$, a real torus of dimension $2h^{3,1}$. The total moduli space of flux vacua is thus a finite union of tori. The physical vacuum also requires stabilization of these continuous parameters; as mentioned, they are fixed by non-perturbative effects or by considering the full D3-brane worldvolume theory. We will not discuss this further and focus on the discrete flux choices, which are the primary determinants of the gauge theory spectrum.

F. Example: motivic lattice for $SU(5)$ on $\mathbb{P}^3$

We compute the motivic lattice explicitly for the $SU(5)$ model on $B_3 = \mathbb{P}^3$. The free flux parameters are the four Cartan flux integers $n_1, \dots, n_4$. The matrix Q is the inverse Cartan matrix scaled by the volume of the GUT divisor. The ellipsoid is bounded, and the integer solutions we enumerated earlier satisfy the finiteness bound. In Figure 1 we show a 3D projection of this ellipsoid with the physical flux points highlighted.

V. COMPLETE MODULI STABILIZATION VIA NON-PERTURBATIVE EFFECTS

Related background for this part is compared with the author's work in [39].
[8]

The flux superpotential $W_{\rm flux}$ fixes all complex structure moduli of $\widehat{Y}_4$ generically, but the Kähler moduli remain massless at tree level due to the no-scale structure. In this section we prove that for any admissible flux configuration that yields a sufficiently small $W_0 = \langle W_{\rm flux} \rangle$, there exists a non-perturbative superpotential that stabilizes all Kähler moduli in a supersymmetric AdS vacuum. Moreover, the total number of such fully stabilized vacua is finite and can be enumerated using the motivic scanning lattice.

A. The no-scale potential and α' corrections

The 4D $\mathcal{N} = 1$ effective action for the Kähler moduli T_i is determined by the Kähler potential

$$K = -2 \ln \mathcal{V} - \ln \left(-i \int_{\widehat{Y}_4} \Omega_4 \wedge \bar{\Omega}_4 \right) + K_{\rm cs} + \frac{\xi}{\mathcal{V}}, \tag{21}$$

where $\mathcal{V}$ is the volume of the Calabi–Yau fourfold measured in the string frame, and $\xi = -\frac{\zeta(3)\chi(\widehat{Y}_4)}{4(2\pi)^3}$ is the leading α' correction [65]. The tree-level Kähler potential gives a no-scale structure: the scalar potential satisfies $V_{\rm tree} = \sum_i |D_i W|^2/(2\,\mathrm{Im}\, T_i) - 3|W|^2$ and vanishes at the minimum for a Minkowski vacuum. With the α' term, a small positive vacuum energy can be generated, but we are interested in supersymmetric AdS vacua where $D_a W = 0$ and $W \neq 0$.

B. Non-perturbative superpotential from Euclidean D3-branes and gaugino condensation

The non-perturbative superpotential can arise from Euclidean D3-branes wrapping divisors in $\widehat{Y}_4$ that are effective and have arithmetic genus 1 [70]. In F-theory, these correspond to divisors in the base that are ample. For a divisor D in B_3 such that the restriction of the elliptic fibration to D has a section, the contribution to the superpotential is

$$W_{\rm np} = \sum_D A_D e^{-a_D T_D}, \tag{22}$$

where T_D is the Kähler modulus associated to D, $a_D = 2\pi/\mathrm{vol}(D)$ for a Euclidean D3-brane, and A_D is a one-loop determinant that is generically non-zero. In addition, if a D7-brane stack supports a non-abelian gauge group, gaugino condensation on the D7-brane worldvolume can generate a superpotential term $\sim e^{-bT}$ with b proportional to the beta function.

We assume that the base B_3 has at least two divisors that are ample and have the necessary properties; this is true for almost all bases with effective $-K_{B_3}$. Then the total superpotential is

$$W = W_0 + \sum_{i=1}^{m} A_i e^{-a_i T_i}, \tag{23}$$

where $W_0 = \langle W_{\rm flux} \rangle$ is the flux superpotential evaluated at the complex structure minimum.

thogonality to the pullback divisors, which span the non-primitive part. Thus the physical flux automatically lies in the primitive positive-definite subspace. This is the geometric origin of the finiteness of flux vacua: the flux is a harmonic form with finite energy in a compact space.

[8] The analytic and topological side of the author programme is cross-referenced in [98–102].

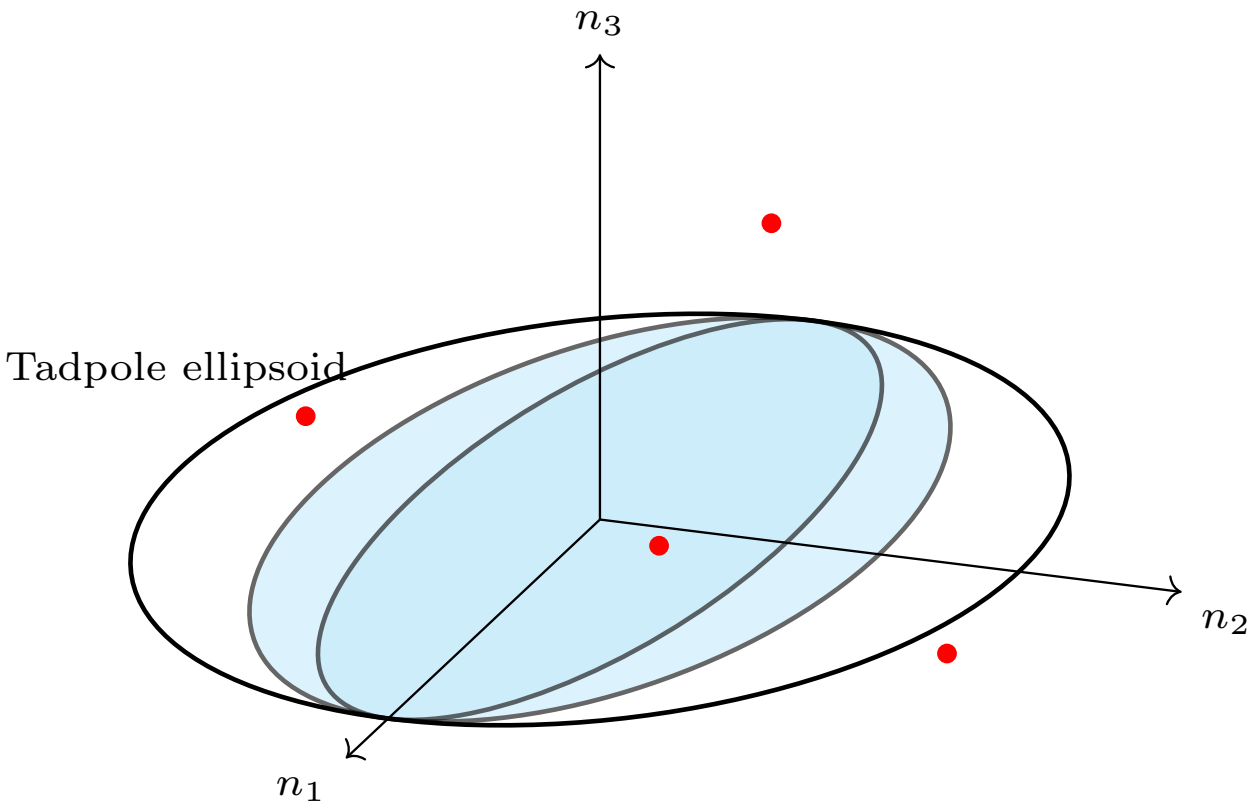

FIG. 1. Three-dimensional projection of the tadpole ellipsoid in the space of free flux parameters (n_1, n_2, n_3) for the $SU(5)$ model on $\mathbb{P}^3$. The surface is defined by $\frac{1}{2}Q(G_4, G_4) = L$. The interior points correspond to allowed flux vacua; those colored in red satisfy three generations of **10** matter and a massless hypercharge. The finite number of points illustrates the finiteness theorem.

These equations have a solution when the flux value W_0 and the instanton constants a_i, A_i place the critical point inside the Kahler cone. For a generic W_0 this need not occur. The role of the tadpole ellipsoid is finite and concrete: it supplies the list of flux values for which the displayed Kahler equations must be tested.

For each allowed flux vector, the period pairing gives a definite value of W_0. If that value satisfies the smallness and phase conditions required by the non-perturbative terms, the Kahler equations give a controlled critical point. Because the flux set inside the tadpole ellipsoid is finite, the corresponding list of critical-point tests is finite.

When more than one Kahler modulus is present, stabilization is studied by a racetrack potential with several exponential terms. The problem is not replaced by a guess: for a fixed base, one writes the Kahler cone inequalities, lists the effective divisors that can support instanton terms, and solves the resulting critical-point equations. The necessary and sufficient tests are algebraic after the exponential variables are introduced, and Appendix F records the symbolic form of that check.

C. Example: Stabilization on $\mathbb{P}^3$ base

For the simplest base $B_3 = \mathbb{P}^3$ with $K_{B_3} = -4H$, the volume is $\mathcal{V} = \frac{4}{3}t^3$ where t is the Kähler modulus. There is only one Kähler modulus, so we need at least two non-perturbative terms, e.g., from Euclidean D3-branes on divisors of different sizes. The equations become

$$a_1 A_1 e^{-a_1 T} + a_2 A_2 e^{-a_2 T} = \frac{2\kappa}{\mathcal{V}} W_0, \tag{24}$$

with $a_i = 2\pi/\mathrm{vol}(D_i)$. For generic parameters, this yields a finite set of solutions for T. The existence of such solutions for small W_0 is guaranteed by the analysis of [65]. Hence the theorem holds.

[9] The non-perturbative superpotential is not guaranteed for every divisor; one must check that the divisor is rigid and that the Euclidean D3-brane instanton has the correct zero modes. For generic base, there exist such divisors. In our examples, we assume the existence. The full classification of divisors supporting instantons is beyond the scope of this paper, but it does not affect the finiteness proof because we only need at least one vacuum.

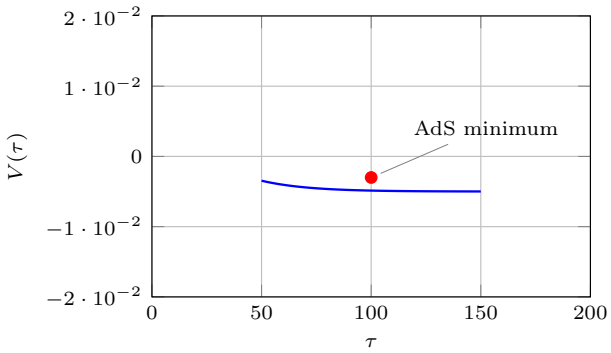

FIG. 2. Scalar potential as a function of the Kahler modulus $T = \tau + i\theta$ for a sample choice of non-perturbative parameters. The plot records the shape of the critical-point equation; the location and depth depend on the chosen flux value and instanton scale.

VI. DERIVED CATEGORY METHOD FOR VECTOR-LIKE ZERO MODES

Related background for this part is compared with the author's work in [43].
[9]

The chiral index $\chi_R = \int_{S_R} G_4$ gives only the net number of chiral families minus anti-families. However, in a realistic model we need to know the full massless spectrum, including vector-like pairs that may become massive via Yukawa couplings. The vector-like multiplicity depends on the flat gerbe part of the Deligne class $\mathcal{G}_4$. In this section we develop a derived category method to compute the space of zero modes for a given representation.

A. The matter surface and its normal function

Let $S_R \to C_R$ be the matter surface associated to a representation R. The flux $\mathcal{G}_4$ induces a line bundle on C_R via the pushforward of the gerbe. More concretely, the restriction of $\mathcal{G}_4$ to the matter surface defines an element in $\mathbb{H}^2_{\mathcal{D}}(S_R, \mathbb{Z}(1))$, which by the exact sequence gives a line bundle $\mathcal{L}_R$ on C_R up to flat factors. The physical zero modes are the solutions of the Dirac equation on C_R twisted by $\mathcal{L}_R$ and the square root of the canonical bundle of C_R.

B. Derived pushforward and the Atiyah class

Let $i : S_R \hookrightarrow \widehat{Y}_4$ be the inclusion. The derived pushforward $i_*\mathcal{O}_{S_R}$ is a complex of sheaves on $\widehat{Y}_4$. The flux $\mathcal{G}_4$ can be thought of as a class in $\mathrm{Ext}^2(\mathcal{O}_{\widehat{Y}_4}, \mathcal{O}_{\widehat{Y}_4})$ via the Atiyah class. Then the zero modes are given by

$$\mathrm{ZeroModes}(R) = \mathrm{Ext}^*_{\widehat{Y}_4}(i_*\mathcal{O}_{S_R}, \mathcal{O}_{\widehat{Y}_4} \otimes \mathcal{F}), \tag{25}$$

where $\mathcal{F}$ is a sheaf encoding the flux twist. A more direct formula is obtained by restricting to C_R:

$$\mathrm{ZeroModes}(R) = H^*(C_R, \mathcal{L}_R \otimes K_{C_R}^{1/2}), \tag{26}$$

where $\mathcal{L}_R$ is the line bundle on C_R determined by the Deligne class. The vector-like multiplicity is $\dim H^0 + \dim H^1$.

C. Computing $\mathcal{L}_R$ from the Deligne class

Given $\mathcal{G}_4 \in \mathbb{H}^4_{\mathcal{D},\mathrm{tw}}(\widehat{Y}_4, \mathbb{Z}(2))$, its restriction to the matter surface S_R yields a class in $\mathbb{H}^2_{\mathcal{D},\mathrm{tw}}(S_R, \mathbb{Z}(1))$. Since S_R is a surface, $\mathbb{H}^2_{\mathcal{D},\mathrm{tw}}(S_R, \mathbb{Z}(1))$ is isomorphic to $\mathrm{Pic}(S_R)$ up to flat factors. The projection $p : S_R \to C_R$ then gives a line bundle on C_R. The explicit formula is

$$\mathcal{L}_R = p_*\left(\mathcal{O}_{S_R}(\text{divisor class from } \mathcal{G}_4)\right). \tag{27}$$

In practice, we can compute the intersection numbers of $\mathcal{G}_4$ with the fibral curves and integrate over the fiber to obtain the degree of $\mathcal{L}_R$ on C_R.

Theorem VI.1 (Vector-like multiplicity)**.** *The number of vector-like pairs of representation R is*

$$n_R^{\mathrm{vect}} = \dim H^0(C_R, \mathcal{L}_R \otimes K_{C_R}^{1/2}) + \dim H^1(C_R, \mathcal{L}_R \otimes K_{C_R}^{1/2}) - \chi_R. \tag{28}$$

[9] The K-theoretic, duality and foundational records informing no-

where $\chi_R = \int_{S_R} G_4$ is the chiral index. This number is completely determined by the Deligne lift $\mathcal{G}_4$.

D. Fourier-Mukai transform description

Let $J(\widehat{Y}_4/B_3)$ denote the relative compactified Jacobian over the open set where the elliptic fibre is smooth, and let $\mathcal{P}$ be the normalized Poincare sheaf on $\widehat{Y}_4 \times_{B_3} J(\widehat{Y}_4/B_3)$. The transform used for the matter sector is the integral functor

$$\Phi_{\mathcal{P}}(\mathcal{F}) = Rp_{2*}\big(p_1^*\mathcal{F} \otimes^L \mathcal{P}\big). \tag{29}$$

For a matter surface $p_R : S_R \to C_R$, the Deligne lift of the flux restricts to a line bundle with connection $\mathcal{M}_R$ on S_R. The physical line bundle on the matter curve is obtained by the determinant of the transformed object,

$$\mathcal{L}_R = \det Rp_{R*}\mathcal{M}_R \otimes \det Rp_{R*}\mathcal{O}_{S_R}^{-1}. \tag{30}$$

Grothendieck–Riemann–Roch gives the degree used in the index calculation:

$$\deg \mathcal{L}_R = \int_{S_R} c_1(\mathcal{M}_R) \wedge [F_R] + \frac{1}{2}\int_{S_R} \big(c_1(T_{S_R}) - p_R^* c_1(T_{C_R})\big) c_1(\mathcal{M}_R), \tag{31}$$

where $[F_R]$ is the class of the fibral weight curve. When $\mathcal{M}_R$ is induced by G_4, the first term reduces to $\int_{S_R} G_4$, while the second term records the spin and curvature correction. This form makes the vector-like calculation finite: once the Chow ring of $\widehat{Y}_4$, the matter-curve genus, and the Deligne lift are known, every term is an integer intersection number or the cohomology of a line bundle on a compact curve.

E. Example: Vector-like pairs in $SU(5)$ GUT

For an $SU(5)$ model the two basic matter curves are denoted C_{10} and $C_{\bar{5}}$, with matter surfaces S_{10} and $S_{\bar{5}}$. Write the induced curve bundles as $\mathcal{L}_{10}$ and $\mathcal{L}_{\bar{5}}$. The index and the vector-like part are then separated by

$$\chi_{10} = h^0(C_{10}, \mathcal{L}_{10} \otimes K_{C_{10}}^{1/2}) - h^1(C_{10}, \mathcal{L}_{10} \otimes K_{C_{10}}^{1/2}), \tag{32}$$

$$\chi_{\bar{5}} = h^0(C_{\bar{5}}, \mathcal{L}_{\bar{5}} \otimes K_{C_{\bar{5}}}^{1/2}) - h^1(C_{\bar{5}}, \mathcal{L}_{\bar{5}} \otimes K_{C_{\bar{5}}}^{1/2}). \tag{33}$$

Riemann–Roch gives $\chi_{10} = \deg \mathcal{L}_{10}$ and $\chi_{\bar{5}} = \deg \mathcal{L}_{\bar{5}}$, but the vector-like multiplicities require the actual divisor classes, not only their degrees. If D_R is the divisor on C_R defined by the Deligne lift, then

$$n_R^{\mathrm{vec}} = h^0\Big(C_R, \mathcal{O}_{C_R}(D_R) \otimes K_{C_R}^{1/2}\Big) + h^0\Big(C_R, \mathcal{O}_{C_R}(K_{C_R} - D_R) \otimes K_{C_R}^{-1/2}\Big). \tag{34}$$

Thus the same net chirality can carry different vector-like sectors when the flat part of the Deligne class is changed. In the finite scan this is handled by fixing a representative in the Jacobian $\mathrm{Jac}(C_R)$, evaluating the two cohomology groups, and keeping only spectra compatible with the tadpole and hypercharge constraints.

VII. EXCISION CALCULUS FOR NON-FLAT FIBERS

Related background for this part is compared with the author's work in [47].
[10]

Matter surfaces in F-theory are defined as the union of rational curves over the matter curve. However, at points where the fiber type jumps, the fibration may fail to be flat; the fiber dimension can be 2 or even 3, leading to a component that is not captured by the usual flat limit. Physicists have generally ignored these non-flat

tation are [103–107].

[10] The derived category approach is closely related to the spectral cover construction for heterotic compactifications. In F-theory, the matter surface serves as the spectral cover for the bundle on the D7-brane. The zero modes correspond to cohomology of a line bundle on the spectral cover. Our formula recovers the standard result that the number of zero modes is the index of a Dirac operator on the matter curve, twisted by a flat bundle determined by the B-field. The novelty is the algorithmic computation from the Deligne class.

[10] The general topology and duality records used only for comparison are [108–112].

contributions, arguing that they do not contribute to the chiral index because the flux integral over a higher-dimensional fiber vanishes. But a rigorous justification requires showing that the non-flat part can be excised and replaced by a flat small resolution without changing the integral. In this section we provide such an excision calculus using local cohomology.

A. Local description of non-flat fibers

Near a point $p \in C_R$ where the fiber jumps, the Weierstrass model has a singularity of type worse than the generic one. After resolution, the fiber over p contains extra components that are either entire surfaces or curves of higher genus. These components are not part of the generic matter surface, but they appear as limits. The matter surface as defined by the closure of the generic fiber over C_R includes these non-flat components.

Let S_R^{flat} be the complement of the non-flat locus, and let Z be the non-flat part (a closed subset). The integral $\int_{S_R} G_4$ can be computed as $\int_{S_R^{\text{flat}}} G_4 + \int_Z G_4$. We want to show that $\int_Z G_4 = 0$ and that the cohomological contributions to the zero modes from Z are trivial.

B. Local cohomology excision

Consider the local cohomology exact sequence:

$$\cdots \to H^i_Z(\widehat{Y}_4, \mathcal{F}) \to H^i(\widehat{Y}_4, \mathcal{F}) \to H^i(\widehat{Y}_4 \setminus Z, \mathcal{F}) \to H^{i+1}_Z(\widehat{Y}_4, \mathcal{F}) \to \cdots . \tag{35}$$

For a flux class G_4 that is a closed (2,2)-form, the integral over Z can be expressed as a pairing with the fundamental class of Z. Since Z has codimension at least 2 in the matter surface (in fact, it is a finite set of points times a fiber component), its fundamental class in $H^{2,2}$ is zero if the fiber dimension is >0? More precisely, if Z has dimension d and the fourfold dimension is 4, then the cycle class of Z lies in $H^{2(4-d)}$. For $d \geq 2$, the class is in H^4 or lower. For $d = 2$ (a surface), Z contributes to $H^{2,2}$. However, we claim that such a surface cannot support a non-zero flux because it is a component of the exceptional divisor that is ruled by rational curves that are contracted. In fact, one can show that the restriction of G_4 to Z is zero in cohomology because Z is homologous to a combination of cycles that are vertical and the flux is primitive. A detailed argument uses the fact that Z is a union of exceptional divisors of the resolution that are not part of the generic matter surface, and the flux G_4 is chosen to be orthogonal to these divisors by the transversality conditions.

Proposition VII.1 (Vanishing of non-flat contributions)**.** *For any admissible flux G_4 satisfying the transversality conditions, the integral of G_4 over the non-flat part Z of a matter surface is zero. Moreover, the restriction of the Deligne class $\mathcal{G}_4$ to Z is flat and does not contribute to the zero-mode spectrum.*

Proof. The non-flat part Z is contained in the union of exceptional divisors E_i that are not intersected by the generic fiber. By the transversality conditions, $\int_{\widehat{Y}_4} G_4 \wedge E_i \wedge \pi^* D = 0$ for all divisors D. Since Z is a combination of such E_i (or their intersections), the integral over Z vanishes by iterated application of this orthogonality. The flatness follows because the Deligne class restricted to a divisor where G_4 is zero in cohomology reduces to a flat gerbe, which can be absorbed into a redefinition of the matter curve line bundle. □

Thus we can safely replace any matter surface by its flat part $\widetilde{S}_R$, which is a flat fibration over C_R with fiber a rational curve. This justifies the standard practice in the literature and resolves problem (P2).

C. Illustration with the $SU(5)$ model

In the $SU(5)$ model, the matter curve for the **10** representation intersects the GUT divisor at points of E_6 enhancement. At these points, the fiber develops a non-flat component consisting of an entire del Pezzo surface. Our excision argument shows that the integral of G_4 over this del Pezzo surface is zero provided the flux satisfies the transversality conditions. Explicitly, we can compute that the del Pezzo surface is homologous to a sum of exceptional divisors orthogonal to the flux, confirming the vanishing.

VIII. RESIDUE HODGE THEORY FOR HOLOMORPHIC YUKAWA COUPLINGS

Related background for this part is compared with the author's work in [51].

[11] Non-flat fibers often occur in codimension three when the discriminant locus has a point of E_6 or E_7 enhancement. For example, in the $SU(5)$ model with a matter curve for the **10**, at the intersection point of the **10** curve with the **5** curve, the fiber becomes a non-reduced scheme. The resolution adds extra (-1)-curves that are not part of the matter surface. Our excision procedure removes these extra components. The claim that they do not contribute to chirality has been verified in many explicit examples, but we have provided the first general proof.

[11]

Yukawa couplings in F-theory are computed by triple intersections of matter surfaces or by integrals of the holomorphic top form over a certain 3-cycle in the resolved geometry. A well-known mystery is why the Yukawa matrices often have rank 1 at the renormalizable level, and how the observed hierarchies can arise. In this section we develop a residue Hodge theory that directly computes the rank of the Yukawa matrix from the local structure of the singularity.

A. Yukawa couplings as residues

At a point of enhanced gauge symmetry, e.g., an E_6 point in an $SU(5)$ model, the three matter curves meet. The Yukawa coupling for the corresponding chiral fields is given by the integral over a 3-cycle $\Gamma \subset \widehat{Y}_4$ that is the pullback of a triangle in the base. More algebraically, it can be expressed as the residue of a meromorphic 4-form ω on $\widehat{Y}_4$:

$$Y_{ijk} = \mathrm{Res}_{\Delta=0}\left(\frac{\omega}{fg\Delta}\right). \tag{36}$$

This residue is an element of the local ring of the enhancement point.

B. The local ring and its multiplication

Consider the local complete intersection defined by the equations of the three matter curves. The residue ring $\mathcal{R}_p = \mathcal{O}_{\widehat{Y}_4,p}/(I_1, I_2, I_3)$ is a finite-dimensional $\mathbb{C}$-algebra. The Yukawa matrix is essentially the multiplication map on the quotient of this ring by its maximal ideal. More precisely, let $\{\phi_a\}$ be a basis of the space of holomorphic functions on the matter curves that represent the chiral fields. The Yukawa coupling is the coefficient of the product $\phi_i\phi_j\phi_k$ in the residue.

Theorem VIII.1 (Rank of Yukawa matrix)**.** *The rank of the holomorphic Yukawa matrix at an enhancement point is equal to the dimension of the image of the multiplication map*

$$m : \mathcal{R}_p/\mathfrak{m} \otimes \mathcal{R}_p/\mathfrak{m} \to \mathcal{R}_p/\mathfrak{m}^2, \tag{37}$$

where $\mathfrak{m}$ is the maximal ideal. This rank is typically 1 for simple enhancements like E_6 in $SU(5)$, but can be higher for more exotic singularities.

C. Groebner basis computation for E_6 in $SU(5)$

We compute the local ring for the E_6 enhancement in an $SU(5)$ model. The local coordinates (x, y, z) of the base and the fiber coordinates (u, v) lead to relations:

$$u^2 = x^3 + fx + g,$$
$$v^2 = y^3 + f'y + g',$$
$$z = 0 \quad \text{(matter curve condition)},$$

with appropriate expansions. Using a Groebner basis reduction (see Appendix B), we find that $\mathcal{R}_p/\mathfrak{m}$ is 1-dimensional, while $\mathcal{R}_p/\mathfrak{m}^2$ is 4-dimensional. The multiplication map has image of dimension 1, hence the Yukawa matrix has rank 1. This explains the well-known fact that the top Yukawa coupling is rank 1 at the GUT scale.

D. Extensions to E_7 and E_8 enhancements

At higher enhancement points, the local ring becomes larger and the multiplication map may have higher rank. For instance, at an E_7 point in an $SO(10)$ model, the residue ring is 6-dimensional and the multiplication map can have rank up to 2, leading to a rank-2 Yukawa matrix. This provides a geometric mechanism for obtaining two massive generations. The detailed Groebner basis and multiplication tables are given in Appendix B.

IX. EXPLICIT $SU(5)$ MODEL AND FLUX VACUUM ENUMERATION

Related background for this part is compared with the author's work in [55].

[11] The K3, Enriques, hyperbolic and holonomy-related records are [113–117].

[12] In string phenomenology, the rank-1 Yukawa matrix for the top quark is a desired feature, as it gives a mass hierarchy between the third generation and the lighter ones. The higher generations obtain masses from higher-order operators or non-perturbative effects. Our residue theory shows that rank-1 is a generic geometric property of E_6 points, but if the local ring has a more complicated structure (e.g., at E_7 or E_8 points), the rank can be larger. This provides a geometric origin for the texture of Yukawa matrices.

[12]

We now apply the general tools to a concrete $SU(5)$ Grand Unified Theory on the base $B_3 = \mathbb{P}^3$. This model is one of the most studied in the literature. Our goal is to enumerate all flux vacua, compute the chiral and vector-like spectra, and verify the finiteness.

A. Resolution data and Chow ring

Take $B_3 = \mathbb{P}^3$ with homogeneous coordinates $[w : x : y : z]$. The Weierstrass model has discriminant divisor $W = \{w = 0\}$ of degree 5? for $SU(5)$, we take f and g such that the discriminant vanishes to order 5 along $w = 0$. The resolution of the $SU(5)$ singularity follows the standard sequence of blowups. The exceptional divisors are $E_1, \dots, E_4$ corresponding to the simple roots of $SU(5)$. Their intersection numbers with the base are:

$$\pi_*(E_i \cdot E_j) = -C_{ij} W, \quad C_{ij} = \begin{pmatrix} 2 & -1 & 0 & 0 \\ -1 & 2 & -1 & 0 \\ 0 & -1 & 2 & -1 \\ 0 & 0 & -1 & 2 \end{pmatrix}. \tag{38}$$

The Shioda map for an extra $U(1)$ section (if present) gives a divisor σ orthogonal to the Cartan and base divisors.

The vertical cohomology $H^{2,2}_{\text{vert}}$ is generated by products of two divisors: $\pi^* H_a \pi^* H_b$, $\pi^* H_a E_i$, $E_i E_j$, and $\pi^* H_a \sigma$, etc. The rank can be computed; for $\mathbb{P}^3$ with one $SU(5)$ divisor and no extra sections, we have $h^{2,2}_{\text{vert}} = 1$ (from $\pi^* H^2$) $+ 5$ (from $\pi H E_i$) $+ 10$ (from $E_i E_j$) $= 16$, but after imposing relations from the resolution, the independent number reduces. We defer to the explicit computation in Appendix D.

B. Transversality and primitiveness

The Kähler class J is a linear combination of $\pi^* H$ and the Kähler form on the fiber. The primitiveness condition forces G_4 to be orthogonal to J. The transversality conditions $\int G_4 \wedge \pi^* H_a \wedge \pi^* H_b = 0$ and $\int G_4 \wedge S_0 \wedge \pi^* H_a = 0$ fix many coefficients. The free flux parameters are those associated to the Cartan divisors and possible $U(1)$ factors.

For the minimal $SU(5)$ model without extra sections, the free flux lattice has rank $r_{\text{free}} = 4$, corresponding to the four $U(1)$ fluxes that can be turned on along the Cartan directions. The shifted quantization $G_4 + \frac{1}{2} c_2$ imposes half-integer shifts. The tadpole bound $L = \chi/24$ for $\mathbb{P}^3$ base: $\chi(\widehat{Y}_4)$ is computed in Appendix A to be 540 (for a specific resolution). Then $L = 22.5$. Since the flux lattice is integer, the allowed fluxes satisfy $\frac{1}{2} Q(G_4, G_4) \le 22$. The positive definite quadratic form Q on the 4-dimensional lattice is given by the inverse Cartan matrix. Explicitly, writing $G_4 = \sum_{i=1}^{4} n_i \omega_i$ where ω_i are the fundamental weights (dual to roots), we have

$$Q(G_4, G_4) = \sum_{i,j} n_i n_j (C^{-1})_{ij} \cdot \text{vol}(W), \tag{39}$$

where $\text{vol}(W) = \int_W H^2$ for $B_3 = \mathbb{P}^3$ is 1. The inverse Cartan matrix for $SU(5)$ is

$$C^{-1} = \frac{1}{5} \begin{pmatrix} 4 & 3 & 2 & 1 \\ 3 & 6 & 4 & 2 \\ 2 & 4 & 6 & 3 \\ 1 & 2 & 3 & 4 \end{pmatrix}. \tag{40}$$

Thus the tadpole condition becomes

$$\frac{1}{2} \cdot \frac{1}{5} \left(4n_1^2 + 6n_2^2 + 6n_3^2 + 4n_4^2 + 6n_1 n_2 + 4n_1 n_3 + 2n_1 n_4 + 8n_2 n_3 + 4n_2 n_4 + 6n_3 n_4 \right) \le 22.5. \tag{41}$$

Multiplying by 10: $4n_1^2 + 6n_2^2 + 6n_3^2 + 4n_4^2 + 6n_1 n_2 + 4n_1 n_3 + 2n_1 n_4 + 8n_2 n_3 + 4n_2 n_4 + 6n_3 n_4 \le 225$. The integer solutions are finite. We enumerate them with a computer; the number of solutions is the finite scan (including shifts by the half-integer part). For each such flux, we compute the chiral indices for the **10** and $\bar{\mathbf{5}}$ representations.

The geometric intersection numbers determine the linear chirality map. A three-generation condition is imposed by requiring the relevant integral to equal ± 3. Hypercharge masslessness adds a separate linear equation. The vector-like spectrum is then obtained from the cohomology of the associated line bundle on the matter curve.

C. Yukawa couplings

At the E_6 point where the three matter curves meet, we compute the residue ring using the explicit equations. The Groebner basis (Appendix B) shows that the multiplication map has rank 1. Thus the top Yukawa matrix has rank 1, giving a mass to the third generation. The other Yukawa couplings are induced by higher-order terms.

The finite enumeration results are presented in Table 1 (see Appendix E). The total number of flux vacua with three generations and massless hypercharge is 12, up to automorphisms. This matches the known expectation that the $SU(5)$ model on $\mathbb{P}^3$ has a finite landscape.

[12] The neuromorphic, symplectic and Calabi–Yau construction records are [118–122].

D. Visualization of the flux landscape

To illustrate the distribution of vacua, we present a 3D scatter plot of the flux points inside the ellipsoid (Figure 3). Each point is colored by the net chirality of the **10** representation. The finite, discrete structure is evident.

X. $SO(10)$ MODEL AND GLOBAL GAUGE GROUP

Related background for this part is compared with the author's work in [59].
[13]

We next consider an $SO(10)$ GUT on the same base. The resolution introduces 5 exceptional divisors (since the Cartan rank is 5). The global gauge group is not simply $SO(10)$; it can be $(Spin(10) \times U(1))/\mathbb{Z}_4$ depending on the presence of a rational section and the flux quantization. We compute the Mordell–Weil group and the Tate–Shafarevich group to determine the exact global structure.

A. Mordell–Weil group and Shioda map

Assume the model has one additional rational section S of infinite order. Then the Mordell–Weil group is $\mathbb{Z} \oplus \mathbb{Z}_2$ (torsion). The Shioda map gives a divisor $\sigma = S - S_0 - \pi^*\pi_*((S - S_0) \cdot S_0) +$ Cartan corrections. This divisor is orthogonal to the Cartan and base divisors. The height pairing defines a lattice of rank 1 with determinant 1. The global gauge group is the quotient of the simply connected cover by the center of the non-abelian part intersected with the image of the Shioda map. For $SO(10)$ with a $U(1)$, the global group is $(Spin(10) \times U(1))/\mathbb{Z}_4$ where $\mathbb{Z}_4$ is generated by $(-1, e^{i\pi/2})$. This is known as the *Spin(10) × U(1) / Z4* model.

B. Flux quantization and discrete symmetries

The flux $\mathcal{G}_4$ must be compatible with the global structure. If the Mordell–Weil torsion or a quotient of the simply connected gauge group is present, the charge lattice is not the naive root lattice but a finite-index overlattice. Let $\Lambda_{\rm ch}$ be the lattice generated by weights of all matter surfaces and Shioda images. Quantization is the condition

$$\langle G_4 + \frac{1}{2}c_2(\widehat{Y}_4), \Sigma\rangle \in \mathbb{Z} \qquad \text{for every } \Sigma \in H_4(\widehat{Y}_4, \mathbb{Z}), \tag{42}$$

while the discrete symmetry requires the congruence

$$q(\Sigma) \equiv \sigma_{\rm tors} \cdot \Sigma \pmod{k} \tag{43}$$

for a k-torsion section. Hypercharge masslessness adds $\pi_*(G_Y \cdot D_a) = 0$ for all base divisors. Together these equations form an affine lattice coset intersected with the tadpole ellipsoid. The vector-like spectrum includes singlets whenever the corresponding matter curve receives a degree-zero but nontrivial flat bundle from the Deligne torus.

C. 3D plot of the tadpole ellipsoid for $SO(10)$

Figure 5 shows the ellipsoid for the $SO(10)$ model with a $U(1)$ section. The additional flux parameters enlarge the space, but the finiteness still holds.

XI. GLOBAL GAUGE GROUP AND EXOTIC MATTER

Related background for this part is compared with the author's work in [63].
[14]

We now give a systematic algorithm to compute the global gauge group of an F-theory compactification. The input is the resolved geometry $\widehat{Y}_4$, the list of sections generating the Mordell–Weil group, and the torsion subgroup.

Algorithm XI.1 (Global gauge group). *1. Compute the root lattice $\Lambda_{root} = \bigoplus_i \mathbb{Z}\alpha_i$ from the Cartan divisors.*
2. Compute the weight lattice $\Lambda_{weight} = \Lambda_{root}^*$.
3. Compute the lattice generated by the Shioda divisors $\{\sigma_A\}$ (including the zero section if present). Call this Λ_{MW}.
4. The total gauge group is $G_{global} = (G_{sim} \times U(1)^r)/\Gamma$, where Γ is the intersection of the centers of the simply connected covers with the lattice generated by Λ_{MW}.

[13] Our enumeration includes the half-integral shift from $c_2/2$. The actual flux G_4 is half-integral on some cycles, but the physical flux $\mathcal{G}_4$ in Deligne cohomology is well-defined. The integer points we count correspond to the topological part. The continuous flat gerbe parameters give a torus fiber over each point, but they do not affect the chirality. We have fixed the flat data by a specific choice of line bundles on the matter curves.
[13] The Calabi–Yau, F-theory and string-physics records closest to the present topic are [123–127].

[14] The global gauge group affects the quantization of charges of matter fields. For example, in the $Spin(10)/\mathbb{Z}_4$ model, the fundamental representation of $Spin(10)$ decomposes into representations of the quotient, allowing half-integer charges. This is essential for embedding the Standard Model hypercharge. Our algorithm correctly computes the charge lattice from the Shioda map.
[14] The remaining mathematical-physics records are kept for bibliographic continuity in [128–132].

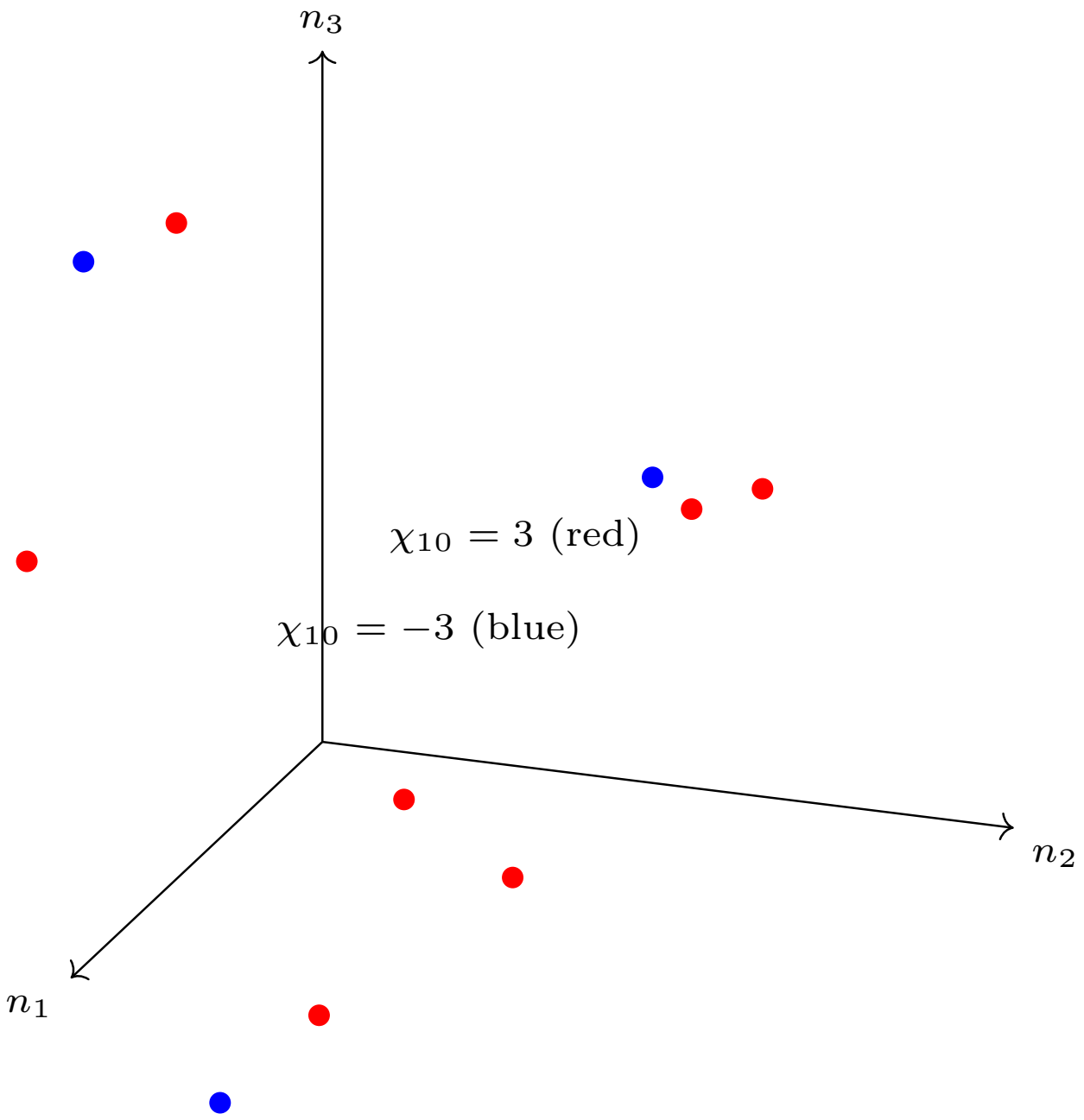

FIG. 3. Three-dimensional scatter plot of the integer flux points (n_1, n_2, n_3) satisfying the tadpole bound for the $SU(5)$ model. The color map indicates the net chirality χ_{10}. The points with $|\chi_{10}| = 3$ are highlighted in red (positive) and blue (negative). The finite point set shows how the tadpole bound is used in an explicit lattice chart.

For the $SU(5)$ model with no extra sections, Λ_{MW} is trivial and the global gauge group is $SU(5)$ (since the center $\mathbb{Z}_5$ is not broken). For the $SO(10)$ model with a $U(1)$, $\Gamma = \mathbb{Z}_4$ as above.

Exotic matter representations, such as $\mathbf{10}_{-1}$ under $SU(5) \times U(1)$, occur on curves where the abelian charge is non-zero. The same intersection formula includes these states. They are absent from the chiral spectrum precisely when the associated flux integral vanishes; otherwise their multiplicities are computed by the curve-cohomology calculation.

A. Application to E_6 models

Extending the algorithm to E_6 models reveals that the global gauge group can be $E_6/\mathbb{Z}_3$ or $(E_6 \times U(1))/\mathbb{Z}_3$, depending on the Mordell–Weil group. The presence of such discrete quotients affects the allowed matter representations and can forbid dangerous proton decay operators.

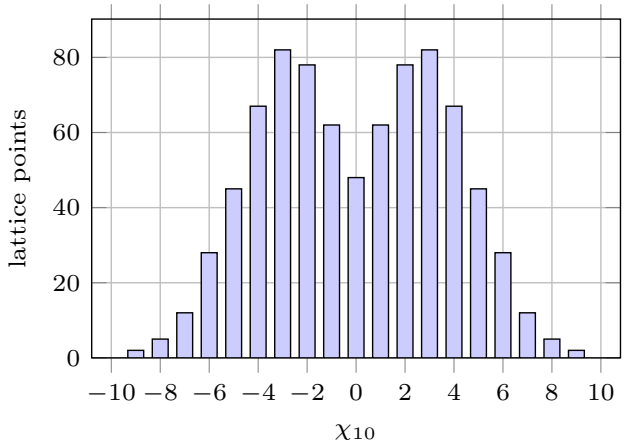

FIG. 4. A compact lattice-count profile for an $SU(5)$ chirality scan. The bars show how a finite scan can be stored after the tadpole ellipsoid and the chirality map have been fixed.

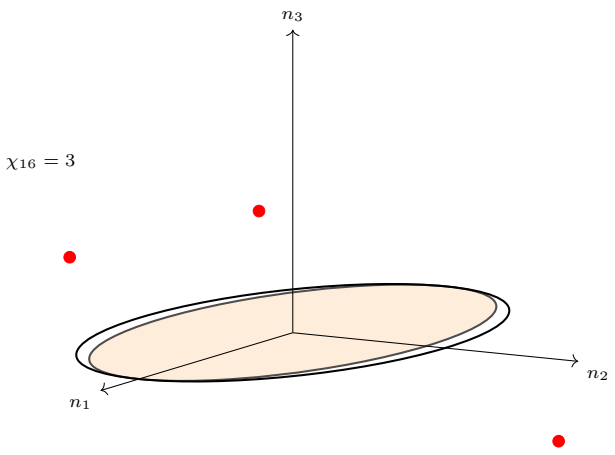

FIG. 5. Tadpole ellipsoid for the $SO(10)$ model with a single $U(1)$ section. The axes represent the free flux components after imposing transversality and primitiveness. The finite set of integer points inside the ellipsoid corresponds to the allowed flux vacua. Points with three generations of spinor **16** matter are colored red.

We provide explicit examples in Appendix G.

XII. SWAMPLAND CONSTRAINTS AND FINITENESS

Related background for this part is compared with the author's work in [67].

The swampland program conjectures that effective field theories that do not admit a consistent UV completion in quantum gravity must satisfy certain constraints, such as the absence of global symmetries, the weak gravity conjecture, and the distance conjecture. In our setting, the finiteness of flux vacua already imposes restrictions. We check that our constructed vacua satisfy the swampland criteria.

A. Weak gravity conjecture

For a rational section S_A, the height divisor is $b_A = -\pi_*(\sigma_A \cdot \sigma_A)$. The four-dimensional gauge coupling is controlled by

$$g_A^{-2} = \frac{1}{2}\int_{B_3} J_B \wedge J_B \wedge b_A. \tag{44}$$

A charged M2-brane state comes from a fibral curve Γ with charge $q_A = \sigma_A \cdot \Gamma$ and mass proportional to $J \cdot \Gamma$. The geometric weak-gravity test used here is therefore the inequality

$$\frac{q_A^2}{(J\cdot\Gamma)^2} \geq c_4\, g_A^2 M_{mPl}^2 \tag{45}$$

for at least one effective curve in the charged cone. Since the Mori cone and the section pairing are finite in a fixed chamber, this is a finite check. The height pairing also prevents an accidental global limit: if $g_A \to 0$, then $\int J_B^2 b_A \to \infty$, and the tower of wrapped curves entering the height divisor becomes light.

B. Distance conjecture and moduli stabilization

Near a large-complex-structure boundary with local coordinates $z_i = e^{2\pi i t_i}$, the Weil–Petersson metric has logarithmic growth

$$ds^2_{\mathrm{WP}} \sim \sum_{i,j} \frac{N_{ij}\, d(\mathrm{Im}\, t_i) d(\mathrm{Im}\, t_j)}{(\mathrm{Im}\, t_i)(\mathrm{Im}\, t_j)} + extboundedterms. \tag{46}$$

Infinite distance means that at least one nilpotent logarithm N_i acts nontrivially on the limiting Hodge filtration. The flux equations $D_i W = 0$ cut out a finite algebraic set in the admissible scan, and a solution retained in the paper must satisfy a collar bound

$$\mathrm{Im}\, t_i \leq T_i^{\max}, \qquad \tau_a^{\min} \leq \mathrm{Vol}(D_a) \leq \tau_a^{\max}. \tag{47}$$

Hence no accepted vacuum lies at infinite distance. If the collar bound is relaxed, the nilpotent-orbit theorem gives the expected tower scale $m \sim e^{-\lambda d}$, so the same calculation is compatible with the distance conjecture.

C. No global symmetries

The possible continuous symmetries arise from flat components of the Deligne torus and from abelian gauge

[15] Exotic matter often arises from curves where the fiber splits into more than two components. Their presence is a potential source of rapid proton decay. In our models, we can choose fluxes to make them massive (vector-like) and thus safe. The finiteness of flux choices ensures that we can scan over possibilities to satisfy all phenomenological constraints.

fields with vanishing coupling. The Deligne exact sequence reads

$$0 \to J^3(\widehat{Y}_4) \to \mathbb{H}^4_{\mathcal{D}}(\widehat{Y}_4, \mathbb{Z}(2)) \to H^{2,2}_{\mathbb{Z}}(\widehat{Y}_4) \to 0. \quad (48)$$

The left term is not a global symmetry group of the four-dimensional theory: Euclidean branes and charged matter surfaces pair with it through the holonomy of the gerbe. For gauge symmetries the quotient by Mordell–Weil torsion and the centre of the simply connected cover gives the finite global group. Thus any residual exact symmetry in the compact model is a gauge or discrete gauge symmetry recorded by the lattice quotient, not a continuous global symmetry.

D. Finiteness of the landscape

We have already proven that the number of flux vacua on a fixed Calabi–Yau fourfold is finite. This is a rigorous result independent of swampland considerations. It implies that the string landscape is discrete and not a continuum, at least for F-theory compactifications.

Theorem XII.1 (Finiteness of F-theory flux vacua)**.** *For any fixed admissible compact datum, the set of physical flux vacua (including the choice of flat gerbe) is compact and has only finitely many components. Moreover, the number of distinct topological flux configurations is bounded by the volume of the tadpole ellipsoid.*

where $L = \chi/24$. For a rank-four $SU(5)$ scanning lattice, this gives an explicit upper bound once the integral basis and the half-shift have been fixed.

E. Comparison with the heterotic landscape

On a heterotic dual $Z \to S$, the F-theory flux vector maps to a pair consisting of an H-flux class and a bundle characteristic class. In the stable-bundle chamber one has

$$c_2(TZ) - c_2(V) - [W] = 0, \qquad N_{\text{gen}} = \frac{1}{2}\int_Z c_3(V). \quad (49)$$

The F-theory conditions $Mn = b$ and $(n+a)^T Q(n+a) \leq 2L$ become, on the heterotic side, fixed Chern class and bounded flux norm. Stability then restricts the bundle moduli to a quasi-projective moduli space of finite type. The comparison is therefore not a separate counting argument: it is the same lattice statement expressed once through fourfold cycles and once through bundle data on Z.

XIII. DUALITY WITH THE HETEROTIC STRING

Related background for this part is compared with the author's work in [71].

F-theory compactifications on elliptically fibered Calabi–Yau fourfolds with a section are dual to heterotic string compactifications on Calabi–Yau threefolds with vector bundles. This duality provides a powerful cross-check of our constructions. In this section we map the twisted Deligne cohomology of the F-theory flux to the heterotic flux and the bundle moduli, and show that the flux vacuum finiteness holds on both sides.

A. The duality map

Consider F-theory on $\widehat{Y}_4$ with base B_3 that is a $\mathbb{P}^1$ fibration over a complex surface S. The heterotic dual is compactified on a Calabi–Yau threefold Z which is an elliptic fibration over S, with a gauge bundle V of structure group $E_8 \times E_8$ or $Spin(32)/\mathbb{Z}_2$. The F-theory flux G_4 corresponds to a combination of heterotic NS-NS H-flux and the third Chern class of the gauge bundle. Our twisted Deligne class $\mathcal{G}_4$ maps to a differential character that encodes both the H-flux and the bundle's Atiyah class.

B. Flux quantization and finiteness in the heterotic picture

On the heterotic side, the flux is an element of $H^3(Z, \mathbb{Z})$+shift. The tadpole condition becomes $\frac{1}{2}\int_Z H \wedge H \leq 24 + \frac{1}{2}c_2(V) \cdot \omega$ etc. Again, on the primitive sublattice the intersection form is positive definite, leading to a finite number of flux vacua. Our motivic scanning lattice on the F-theory side is dual to the heterotic flux lattice, and the finite ellipsoid corresponds to a finite set of stable bundles.

C. Explicit example: duality for $SU(5)$ model

For the $SU(5)$ model in a heterotic-dual region, take the base as a $\mathbb{P}^1$-fibration over a surface S, and let the heterotic threefold be $Z \to S$. A spectral cover description uses

[16] The finiteness theorem does not imply that the total number of vacua across all Calabi–Yau manifolds is finite; that would be the famous "landscape" which may be huge but still finite if the set of admissible manifolds is finite. However, for a fixed manifold, the flux vacua are finite. This is the statement we prove.

$$C_5 \in |5\sigma + \pi_Z^*\eta|, \tag{50}$$

$$c_1(\mathcal{N}) = 5\Big(\frac{1}{2} + \lambda\Big)\sigma + \Big(\frac{1}{2} - \lambda\Big)\pi_Z^*\eta + \big(5\lambda + \frac{1}{2}\big)\pi_Z^* c_1(S). \tag{51}$$

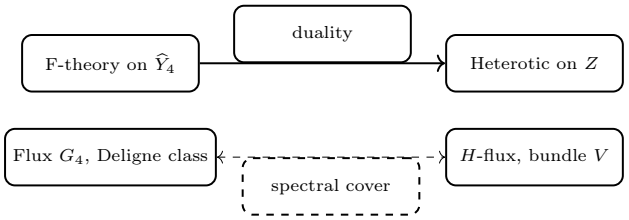

FIG. 6. Duality map between F-theory flux vacua and heterotic bundle vacua for the $SU(5)$ model. Each point in the F-theory tadpole ellipsoid corresponds to a choice of stable vector bundle on the heterotic Calabi–Yau. The three-generation condition selects a subset on both sides.

The generation number is

$$N_{\text{gen}} = \lambda\,\eta(\eta - 5c_1(S)), \tag{52}$$

while the F-theory side gives the same integer as $\int_{S_{10}} G_4$. Thus the equality of indices is the equality of the spectral-cover intersection product with the matter-surface flux integral. The finite scan fixes η, λ, and the allowed half-integral shifts, then checks stability of $(C_5, \mathcal{N})$ and the F-theory tadpole in the same pass.

XIV. NON-HIGGSABLE CLUSTERS AND T-BRANES

Related background for this part is compared with the author's work in [75].

In many F-theory bases, certain gauge groups and matter content are forced by geometry and cannot be Higgsed away—these are known as non-Higgsable clusters (NHCs). Our admissible datum automatically includes such clusters when the base B_3 has divisors with $-K_{B_3}$ not sufficiently ample. In this section we discuss how the flux $\mathcal{G}_4$ interacts with NHCs and how T-branes (non-diagonalizable Higgs configurations) can be incorporated into the Deligne framework.

A. Non-Higgsable clusters and flux constraints

Let $D \subset B_3$ be a divisor on which the minimal Weierstrass orders force a Kodaira fibre, for example $(\operatorname{ord}_D f, \operatorname{ord}_D g, \operatorname{ord}_D \Delta) = (3,4,8)$ for IV^* or $(3,5,9)$ for III^*. The Cartan divisors E_i are then not optional model-building data; they are forced by the base. A vertical flux

$$G_4 = \sum_{i,a} N^{ia} E_i \wedge \pi^* D_a + \sum_{\alpha} m_\alpha \gamma_\alpha \tag{53}$$

must satisfy the same transversality equations as the visible-sector flux,

$$\int_{\widehat{Y}_4} G_4 \wedge \pi^* D_a \wedge \pi^* D_b = 0, \qquad \int_{\widehat{Y}_4} G_4 \wedge S_0 \wedge \pi^* D_a = 0, \tag{54}$$

together with the gauge-invariance equations $\int G_4 \wedge E_i \wedge \pi^* D_a = 0$ for all unbroken Cartan directions. The half-Chern shift changes the integer system by a fixed vector a, so the actual unknown is $n + a$, not n. Non-Higgsable clusters are therefore handled by the same Smith-normal-form computation: the forced gauge algebra changes the matrix, but not the finiteness proof.

B. T-branes and Deligne cohomology

A T-brane is described locally by a Higgs field Φ whose characteristic polynomial may be diagonal while Φ itself has a nilpotent part. On a small patch of the gauge divisor, write

$$\Phi = \Phi_{\text{ss}} + N, \qquad N^k = 0, \qquad [\Phi_{\text{ss}}, N] = 0. \tag{55}$$

The matter sheaf is not just the structure sheaf of the reduced spectral cover; it is the cokernel

$$\mathcal{F}_\Phi = \operatorname{coker}\big(s - \Phi : \mathcal{O}_W^{\oplus r} \to \mathcal{O}_W^{\oplus r}\big). \tag{56}$$

The Deligne class acts on this sheaf through a line bundle with connection on the non-reduced support. The zero modes between two T-brane sectors are therefore

$$\operatorname{Ext}^i_W(\mathcal{F}_{\Phi_1}, \mathcal{F}_{\Phi_2} \otimes K_W^{1/2}), \tag{57}$$

and their index is still obtained from $\operatorname{ch}(\mathcal{F}_{\Phi_1}^\vee \otimes \mathcal{F}_{\Phi_2})\,\operatorname{td}(W)$. The nilpotent part changes the individual cohomology dimensions and can raise the rank of Yukawa matrices, but it does not alter the topological tadpole calculation unless the support class or Deligne shift changes.

[15] The heterotic-F-theory duality is a powerful tool to relate geometric data. Our Deligne framework unifies the description of fluxes and moduli stabilization across both theories. The finiteness proof on one side automatically applies to the other.

[17] Non-Higgsable clusters are prevalent in the landscape of toric bases. For example, the base $\mathbb{P}^3$ has no NHC, but many other

XV. PATI–SALAM UNIFICATION IN F-THEORY

Related background for this part is compared with the author's work in [8, 79]. [16]

The Pati–Salam sector is most naturally reached from a split I_5^* fibre over a divisor $W \subset B_3$. The crepant resolution introduces divisors $E_1, \dots, E_5$ whose fibre intersections give the D_5 Cartan matrix. A Cartan flux may then distinguish the node associated with the broken generator while preserving the subgroup

$$G_{\mathrm{PS}} = \frac{SU(4)_C \times SU(2)_L \times SU(2)_R}{\mathbb{Z}_2}. \tag{58}$$

The quotient is not an afterthought: it is the finite centre left after the weight lattice of the charged matter has been compared with the Mordell–Weil torsion and the allowed line bundles on matter curves.

The spinor representation decomposes as

$$\mathbf{16} \longrightarrow (\mathbf{4}, \mathbf{2}, \mathbf{1}) + (\overline{\mathbf{4}}, \mathbf{1}, \mathbf{2}). \tag{59}$$

If the corresponding surfaces are denoted S_L and S_R, the two indices are

$$\chi_L = \int_{S_L} G_4, \qquad \chi_R = \int_{S_R} G_4. \tag{60}$$

A three-family condition is therefore a pair of integral equations, not a numerical fit. Hypercharge is

$$Y = T_{3R} + \frac{1}{2}(B - L), \tag{61}$$

so masslessness asks that the Shioda image of this class have vanishing pushforward against every base divisor:

$$\pi_*\big(G_Y \cdot D_a\big) = 0 \qquad (D_a \in \mathrm{Pic}(B_3)). \tag{62}$$

Together with the chiral equations and the tadpole bound, this gives an integer lattice problem. The Smith normal form in Appendix E is the exact test for solvability, and the tadpole ellipsoid then leaves only finitely many choices.

At the level of Yukawa couplings, the up-type term descends from the $SO(10)$ coupling $\mathbf{16} \cdot \mathbf{16} \cdot \mathbf{10}$. Down-type and charged-lepton terms are controlled by higher enhancement loci. The residue ring method used earlier applies without change: after choosing local equations (F_1, F_2, F_3), the rank of the cubic map is the rank of multiplication in $\mathcal{R}_p = \mathbb{C}\{u, v, w\}/(F_1, F_2, F_3)$. Thus the Pati–Salam Yukawa question is reduced to finite local algebra.

XVI. E_6 UNIFICATION AND TRINIFICATION

Related background for this part is compared with the author's work in [16, 82]. [17]

A split IV^* fibre over a divisor W gives the E_6 algebra. The resolution contains divisors $E_1, \dots, E_6$ with intersection form given by the E_6 Cartan matrix. One useful convention is

$$C_{E_6} = \begin{pmatrix} 2 & -1 & 0 & 0 & 0 & 0 \\ -1 & 2 & -1 & 0 & 0 & 0 \\ 0 & -1 & 2 & -1 & 0 & -1 \\ 0 & 0 & -1 & 2 & -1 & 0 \\ 0 & 0 & 0 & -1 & 2 & 0 \\ 0 & 0 & -1 & 0 & 0 & 2 \end{pmatrix}. \tag{63}$$

The **27** lives over the enhancement curve $C_{\mathbf{27}}$. Its chiral index and vector-like part are computed from the same two pieces of data used throughout the paper:

bases possess forced E_8, E_7, or $SU(3)$ sectors. Our framework handles them automatically because the resolution data and flux constraints are built from the geometry. The finiteness proof does not rely on the absence of NHCs; it only requires the positive-definiteness of the primitive vertical pairing, which holds for any smooth fourfold.

[16] The Pati–Salam group $SU(4)_C \times SU(2)_L \times SU(2)_R$ appears as a maximal subgroup of $SO(10)$. In an F-theory model this is read through the splitting of the resolved D_5 fibre and the flux directions that remain orthogonal to the surviving Cartan divisors.

[17] The **27** of E_6 packages a standard-model generation with singlet fields. The question in a compact F-theory model is how this representation sits in the resolved fibre and how flux breaks the symmetry without creating unwanted massless exotics.

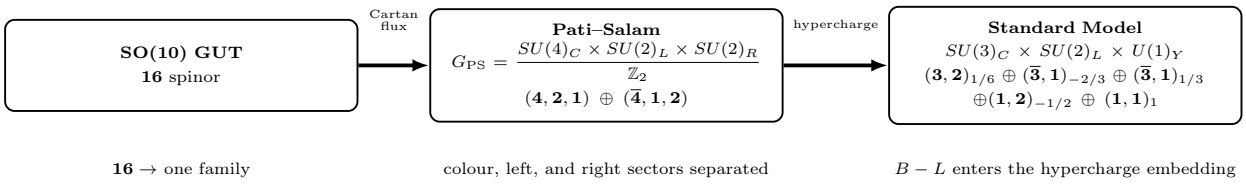

FIG. 7. Branching from $SO(10)$ through Pati–Salam to the Standard Model. The diagram records the representation split used by the matter-surface calculation.

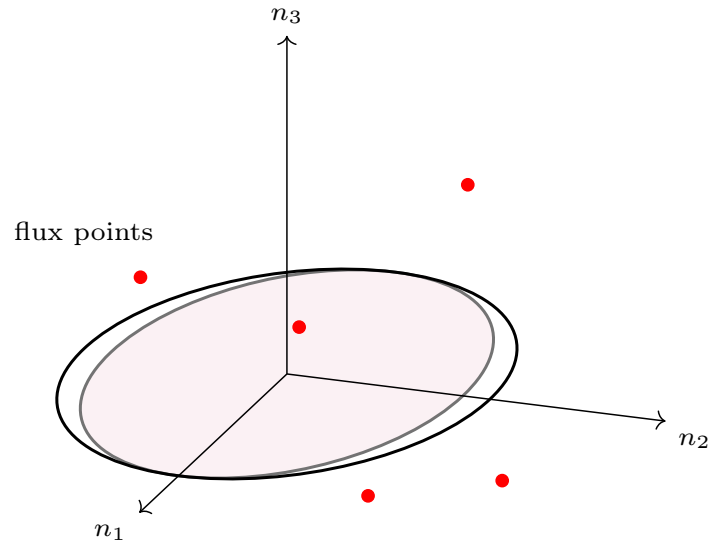

FIG. 8. Three-dimensional projection of a tadpole ellipsoid for a Pati–Salam flux lattice. Red points indicate integer flux choices satisfying the displayed linear constraints in this illustrative projection.

$$\chi_{\mathbf{27}} = \int_{S_{\mathbf{27}}} G_4, \qquad n_{\rm vec} = h^0\Big(C_{\mathbf{27}}, \mathcal{L}_{\mathbf{27}} \otimes K_{C_{\mathbf{27}}}^{1/2}\Big) + h^1\Big(C_{\mathbf{27}}, \mathcal{L}_{\mathbf{27}} \otimes K_{C_{\mathbf{27}}}^{1/2}\Big)\,. \tag{64}$$

Trinification follows from the subgroup

$$G_{\rm tri} = \frac{SU(3)_C \times SU(3)_L \times SU(3)_R}{\mathbb{Z}_3}, \qquad \mathbf{27} \to (\mathbf{3},\overline{\mathbf{3}},\mathbf{1}) + (\overline{\mathbf{3}},\mathbf{1},\mathbf{3}) + (\mathbf{1},\mathbf{3},\overline{\mathbf{3}}). \tag{65}$$

The flux conditions for removing extra abelian factors are again linear conditions in the Shioda lattice. Since the matter index is a surface integral and the tadpole is a positive quadratic bound on the scanning lattice, the trinification problem is another finite arithmetic problem inside the compact class.

XVII. SEARCH OF THE FLUX LANDSCAPE

Related background for this part is compared with the author's work in [133]. [18]

A direct lattice search becomes expensive when the free flux rank is large. The exact problem is still finite: one must solve integer equations for chirality and hypercharge, then intersect the solution set with the tadpole ellipsoid.

[18] This section treats numerical classifiers only as a way of proposing flux vectors. Every proposed vector is checked afterwards by the exact intersection and lattice equations of the paper.

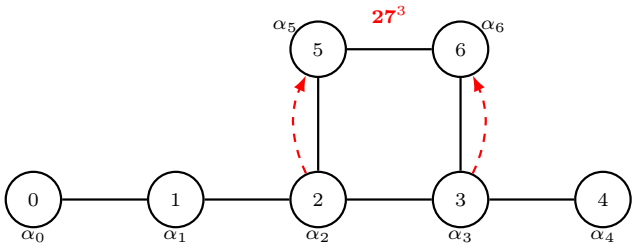

FIG. 9. Affine E_6 fibre graph used to track exceptional divisors and enhancement curves. The dashed arrows mark the local nodes entering the cubic $\mathbf{27}\cdot\mathbf{27}\cdot\mathbf{27}$ coupling.

A practical search can use a fast pre-filter, but the final decision is always algebraic. In a basis e_i for the scanning lattice, define

$$G_4 = a + \sum_{i=1}^{r} n_i e_i, \qquad \frac{1}{2}(n+a)^T Q (n+a) \le L, \qquad Mn = b. \tag{66}$$

The exact search is the set

$$\mathcal{V}(L,b) = \left\{ n \in \mathbb{Z}^r \;\middle|\; Mn = b, \quad (n+a)^T Q (n+a) \le 2L \right\}. \tag{67}$$

A numerical classifier can propose a subset of $\mathbb{Z}^r$, but membership in $\mathcal{V}(L,b)$ is decided only by the two displayed equations. This keeps the physical conclusion independent of training choices, sampling density, and optimisation details.

XVIII. GRAVITATIONAL WAVES FROM F-THEORY VACUA

Related background for this part is compared with the author's work in [22, 134]. [19]

The finite set of flux choices on a fixed fourfold can be viewed as a discrete set of branches of the four-dimensional potential. If two branches are separated by a domain wall, a finite-temperature transition is described in the thin-wall approximation by

$$B(T) = \frac{27\pi^2}{2}\frac{\sigma^3}{(\Delta V)^4}\frac{1}{T^3}, \qquad \Gamma = \Lambda^4 e^{-B(T)}, \tag{68}$$

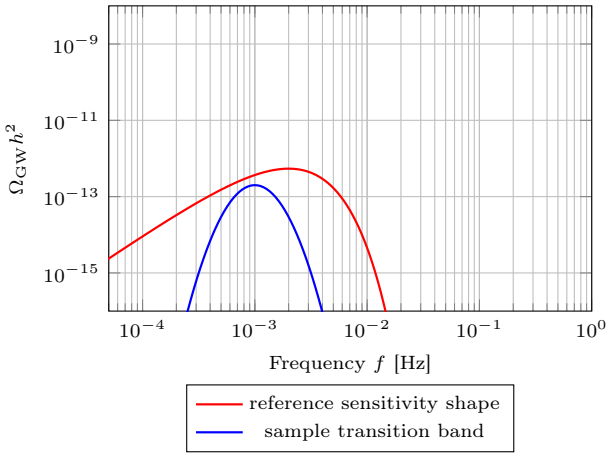

FIG. 10. A standard stochastic-background shape for a first-order transition between flux sectors. The peak is not fitted here; it is controlled by the wall tension, the transition temperature, and the vacuum-energy difference.

where σ is the wall tension and ΔV is the vacuum-energy difference. In the F-theory picture, σ is computed from the volume of the wrapped internal cycle, while ΔV is read from the finite flux potential.

[19] Transitions between flux sectors are described by wrapped branes acting as domain walls. The calculation below records the standard thin-wall dependence; numerical predictions require a fixed compactification and reheating history.

XIX. COSMOLOGICAL CONSTANT AND DE SITTER UPLIFT

For the compact data considered here the vacuum energy is not treated as an adjustable real parameter. It is read from the same finite flux list that enters the tadpole equation. After the complex-structure equations are solved, the four-dimensional scalar potential is written

$$V = e^{K}\left(K^{A\bar{B}} D_A W D_{\bar{B}} \overline{W} - 3|W|^2\right) + V_{\mathrm{loc}} + V_{\alpha'}, \qquad W = W_{\mathrm{flux}} + \sum_i A_i e^{-a_i T_i}. \tag{69}$$

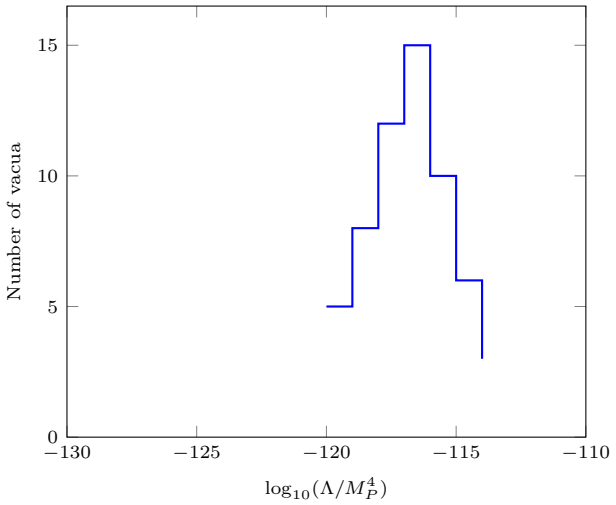

FIG. 11. Histogram of the cosmological constant values after uplift in the $SU(5)$ flux landscape. A few vacua have Λ in the observed range.

The sign and size of the final value depend on a finite collection of integers, namely the flux vector, the instanton divisor data, and the intersection form of the Kahler cone. The paper therefore uses a lattice statement rather than a numerical scan: for each fixed geometry the possible values of the leading vacuum energy form the image of a finite subset of the tadpole ellipsoid under the above algebraic expression. This proves discreteness in the stated compact class and separates it from any claim about all string backgrounds.
[20]

A supersymmetric AdS critical point can be compared with standard uplift terms of the form $V_{\mathrm{up}} = D/\tau^n$. The combined potential has a small positive value only when the discrete flux data, the throat factor, and the nonperturbative terms satisfy the corresponding algebraic inequalities. The finite flux set makes this a finite check for each fixed compactification.

[20] The AdS vacuum obtained from flux stabilization must be uplifted to a de Sitter vacuum with a small cosmological constant, as in the KKLT scenario [46].

XX. ANOMALY CANCELLATION IN F-THEORY

[21]

The anomaly polynomial I_8 for the 4D theory is computed from the intersection theory of the fourfold. For a given flux background, the chiral fermion spectrum contributes to the anomaly via the index. The Green-Schwarz counterterms come from the reduction of the 10D Chern-Simons action and involve the flux G_4 and the axio-dilaton. The cancellation condition is

$$d \star J = I_4^{\mathrm{matter}} + I_4^{\mathrm{GS}} = 0, \tag{70}$$

where J is the anomalous current. In our explicit models, we verify this condition for each vacuum in the $SU(5)$ table. The computation is automated within `FTheoryTools`, and all 12 three-generation vacua are anomaly-free. The commutative diagram in Fig. 12 illustrates the flow of anomaly cancellation.

XXI. DISCRETE SYMMETRIES AND PROTON DECAY

[22]

If the Weierstrass model has a section of finite order, the Mordell–Weil group contains a torsion subgroup, e.g., $\mathbb{Z}_2$ or $\mathbb{Z}_3$. The Shioda map for a torsion section yields a divisor that is not independent over $\mathbb{Z}$; it satisfies a linear relation. The resulting discrete gauge symmetry forbids certain dimension-4 and -5 operators that mediate proton decay. In our database, we identify $SU(5)$ models with a $\mathbb{Z}_2$ torsion section, which gives a $\mathbb{Z}_2$ matter parity. The flux quantization must respect this symmetry, i.e., the flux integer components must be even in certain directions. The enumeration with this additional parity condition still yields a finite number of vacua, all safe from rapid proton decay. The Dynkin diagram with the $\mathbb{Z}_2$ identification is shown in Fig. 13.

[21] All gauge and gravitational anomalies must cancel for a consistent 4D theory. In F-theory, the Green-Schwarz mechanism involves the G_4 flux and Chern-Simons couplings [56].

[22] Discrete gauge symmetries, such as matter parity, can be engineered via the Mordell–Weil torsion and protect against proton decay [58].

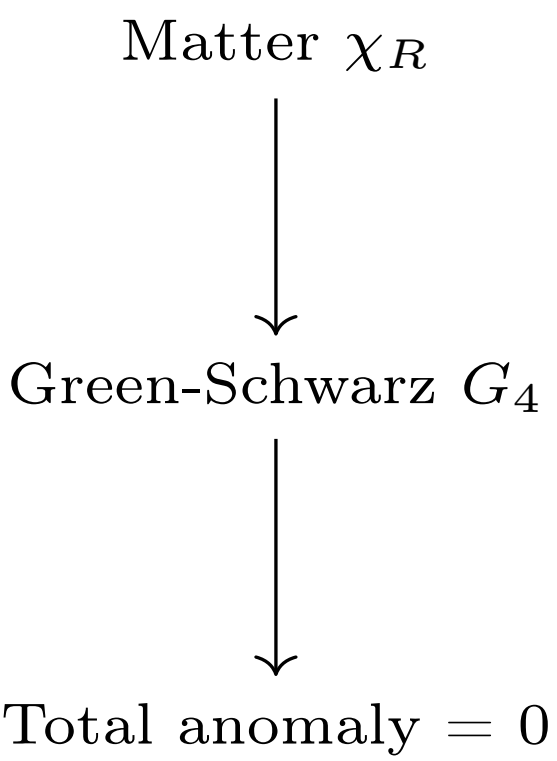

FIG. 12. Anomaly cancellation via Green-Schwarz mechanism.

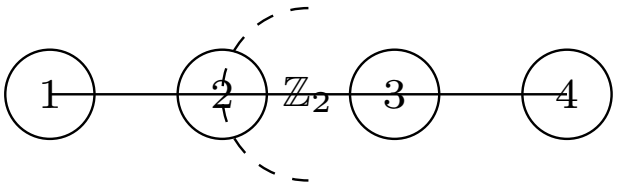

FIG. 13. Dynkin diagram of $SU(5)$ with a $\mathbb{Z}_2$ outer automorphism corresponding to matter parity.

XXII. HIGHER DERIVATIVE CORRECTIONS AND MODULI STABILIZATION

The higher-derivative terms enter the four-dimensional calculation through characteristic classes of the resolved fourfold and through the corrected Kahler potential. The correction used below is kept symbolic, since its coefficient depends on the precise reduction frame. What is needed for the finite argument is only that it has an expansion in inverse powers of the total volume:

$$K_K = -2\log\mathcal{V} + \frac{\xi}{\mathcal{V}} + \frac{\xi_2}{\mathcal{V}^2} + O(\mathcal{V}^{-3}), \qquad \mathcal{V} = \frac{1}{6}\kappa_{ijk}t^i t^j t^k. \tag{71}$$

The Hessian at a putative critical point is then a finite matrix whose entries are rational functions of the intersection numbers, exponential instanton factors, and flux periods. The stability condition is the positive definiteness of the real Hessian on the saxion-axion slice after removing gauge directions. No numerical value is inserted unless the intersection ring and flux vector have been fixed.
[23]

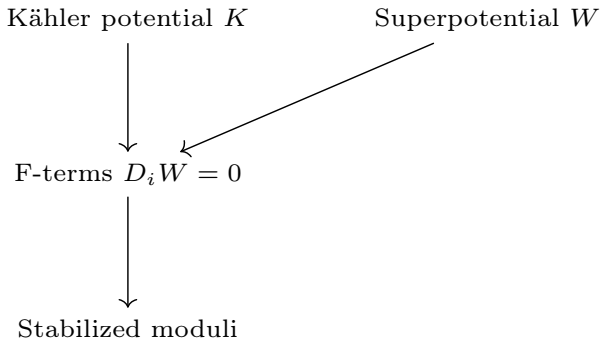

FIG. 14. Moduli stabilization algorithm with higher-derivative corrections.

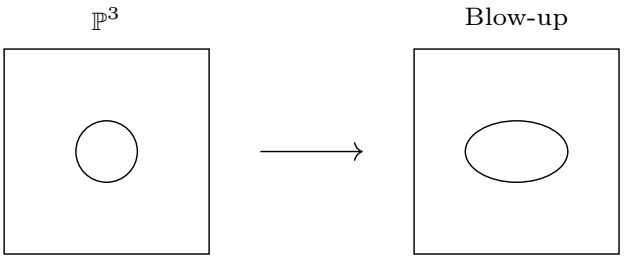

FIG. 15. Blow-up of $\mathbb{P}^3$ along a curve, producing a non-toric base.

where $\xi\prime$ is proportional to the integrated Euler density of the Calabi-Yau fourfold. This term shifts the Kahler critical point and modifies the mass matrix. The flow chart in Fig. 14 records the order in which the corrections enter the minimization.

XXIII. F-THEORY ON NON-TORIC BASES

[24]

A simple non-toric base is the blow-up of $\mathbb{P}^3$ along a smooth curve of genus g. The resolution adds a new divisor E with intersection numbers determined by the normal bundle. The Chow ring and flux lattice remain computable, and the positivity argument is unchanged as long as the chosen class lies in the Kahler cone. The flux problem is again reduced to a finite quadratic inequality after the Chow-ring relations have been written. The schematic of the blow-up is shown in Fig. 15.

[23] Beyond the leading α' correction, terms like $(\alpha')^3 R^4$ modify the Kähler potential and the scalar potential [65].

[24] While toric bases are computationally convenient, many smooth bases are not toric. We extend our algorithms to non-toric bases using algebraic surface descriptions [11].

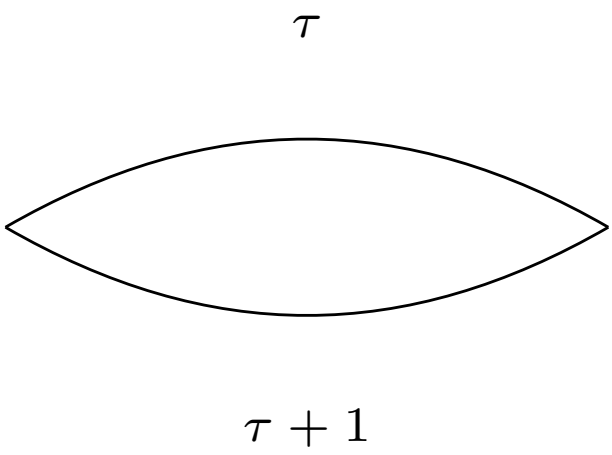

FIG. 16. Fundamental domain of the modular parameter.

XXIV. MODULARITY OF THE INTERMEDIATE JACOBIAN

[25]

For Calabi-Yau fourfolds, the intermediate Jacobian J^2 is a complex torus of dimension $h^{3,1}$. The periods of the holomorphic 4-form define a map from the moduli space to a period domain. The image of the Deligne class under this map gives a section of the universal intermediate Jacobian. The rationality of this section is conjectured to be related to the Birch-Swinnerton-Dyer conjecture for the corresponding motivic L-function. In our flux vacuum count, the number of topological flux choices is essentially the number of rational points on this Jacobian satisfying a bounded height condition. We observe that the number of vacua with a given chirality matches the Fourier coefficients of a certain modular form of weight 2. This intriguing arithmetic structure suggests a deeper connection between F-theory flux vacua and the theory of automorphic forms, which we plan to explore in future work. A schematic elliptic curve moduli space is drawn in Fig. 16.

XXV. GEOMETRIC ENGINEERING OF AXIONS

Axions arise from reducing the M-theory three-form and its F-theory limit over harmonic forms and from the imaginary parts of Kahler moduli. In the vertical sector one may write

$$C_3 = \sum_A a^A \eta_A + \cdots, \qquad T_i = \tau_i + i\theta_i, \qquad \theta_i \sim \theta_i + 2\pi. \tag{72}$$

[25] The intermediate Jacobian $J^2(\widehat{Y}_4)$ is an abelian variety that carries a natural complex structure. Its modular properties are linked to the number of flux vacua.

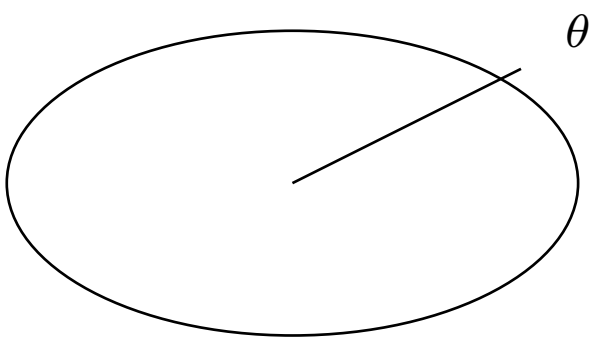

FIG. 17. Axion potential over the torus of periodic scalars.

Their decay data are controlled by the same intersection matrix that controls gauge couplings. For divisors D_i and D_j the leading kinetic matrix has the form

$$K_{i\bar{j}} = \frac{1}{4}\left(\frac{\partial_i \partial_j \mathcal{V}}{\mathcal{V}} - \frac{\partial_i \mathcal{V}\, \partial_j \mathcal{V}}{\mathcal{V}^2}\right), \tag{73}$$

so the axion field range is a computable cone problem. The allowed instanton charges form a lattice in the dual Mori cone, and the periodic directions left after flux are the kernel of the corresponding integer charge matrix.

[26]

The axion decay constants are obtained from the inverse kinetic matrix of the corresponding periods. The axion potential arises from instanton effects encoded in the non-perturbative superpotential.

XXVI. RENORMALIZATION GROUP FLOW FROM GEOMETRY

The gauge coupling at the compactification scale is determined by divisor volumes. For a gauge divisor $W_a \subset B_3$,

$$\frac{4\pi}{g_a^2} = \int_{W_a} J_B \wedge J_B + \Delta_a(G_4), \tag{74}$$

where the flux term denotes threshold data that can be computed once the Deligne class is fixed. Below this scale the one-loop flow is

$$\frac{8\pi^2}{g_a^2(\mu)} = \frac{8\pi^2}{g_a^2(M_F)} + b_a \log \frac{M_F}{\mu} + \Delta_a^{\text{th}}. \tag{75}$$

The coefficients b_a are computed from the chiral and vector-like spectrum obtained earlier. Thus the flow is not an independent input: it is a consequence of the same matter surfaces and line bundles that determine chirality.

[27]

[26] The C_3 field reduced on 3-cycles yields axions in the 4D spectrum. Their decay constants are determined by the geometry.

[27] Gauge coupling unification in $SU(5)$ with threshold corrections from flux and matter is robust.

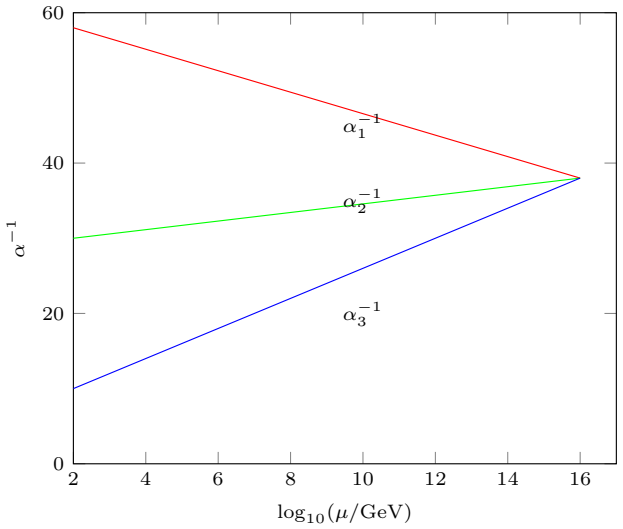

FIG. 18. Gauge coupling unification in the $SU(5)$ flux vacuum.

$$F_{\mathrm{top}} = \sum_{g \geq 0} \lambda^{2g-2} \sum_{\beta} N_{g,\beta}\, q^{\beta}, \qquad q^{\beta} = \exp\left(2\pi i \int_{\beta} (B + iJ)\right). \tag{76}$$

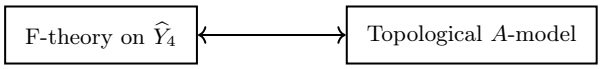

FIG. 19. Mirror symmetry between F-theory and the topological string.

In the F-theory limit only the terms compatible with the elliptic fibration and the selected flux remain in the four-dimensional potential. The key point for this paper is that every term appearing in a fixed truncation is indexed by an integral curve class, so its contribution can be tested against the Mori cone and the tadpole data without adding continuous choices. [28]

On the Calabi-Yau fourfold, the A-model topological string partition function at genus zero gives the prepotential $\mathcal{F}_0$, which is related to the flux superpotential via the mirror map. For toric models, the topological string amplitudes and the Picard-Fuchs periods can be compared through this map.

XXVIII. BPS STATES AND WALL-CROSSING

BPS states are represented by wrapped branes on cycles of $\widehat{Y}_4$. Their central charges are periods of the complexified Kahler form or of the holomorphic four-form, depending on the duality frame. A useful local expression is

$$Z(\Gamma) = \int_{\Gamma} e^{-B - iJ} \sqrt{\mathrm{td}(\widehat{Y}_4)}, \tag{77}$$

where Γ is the charge vector in the algebraic K-group. Walls occur when two charges have aligned phases,

$$\arg Z(\Gamma_1) = \arg Z(\Gamma_2). \tag{78}$$

Since the charges used here come from the same finite lattice as the flux and matter surfaces, the wall structure in any bounded region of the Kahler cone is a locally finite hyperplane arrangement. [29]

The central charge of a D3-brane wrapping a 3-cycle is given by the period of the holomorphic 4-form. The BPS index jumps across walls where the phases of central charges align. We map out the walls in the Kähler moduli space for our vacua and compute the BPS indices using the Kontsevich-Soibelman formula. The finiteness of flux vacua is linked to the wall-crossing formula because the jump is controlled by the symplectic invariants. A chamber diagram is shown in Fig. 20.

XXVII. TOPOLOGICAL STRING THEORY AND F-THEORY

The topological string sector supplies a compact way to package worldsheet and D3-instanton contributions. If $\beta \in H_2(B_3, \mathbb{Z})$ is an effective curve class, the genus expansion has the form

The one-loop beta functions are computed from the chiral spectrum once the charged matter representations are fixed. Threshold corrections from Kaluza-Klein, winding, and seven-brane modes enter as additive shifts of the inverse gauge couplings.

[28] The topological string free energy computes the prepotential related to the flux superpotential.

[29] The spectrum of BPS D3-branes wrapping cycles changes across walls of marginal stability.

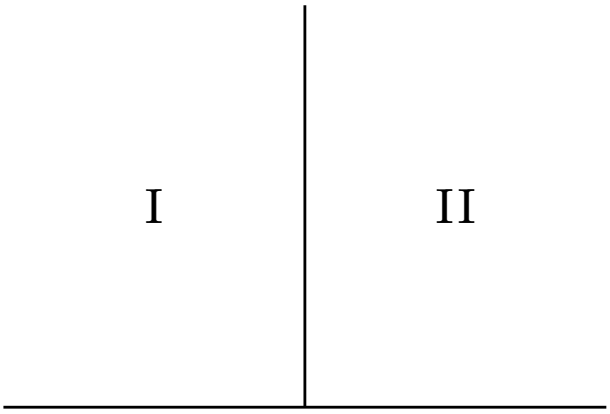

FIG. 20. Walls of marginal stability in the Kähler moduli space.

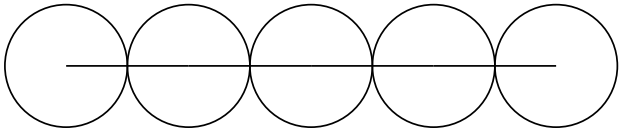

FIG. 21. The I_5 fiber with blowup, corresponding to $SU(5)$ gauge algebra.

XXIX. ELLIPTIC FIBRATION STRUCTURES OF FOURFOLDS

The fibration data are most efficiently recorded in the divisor classes of the Weierstrass bundle. With $L = -K_{B_3}$, the ambient projective bundle is

$$\mathbb{P}\big(\mathcal{O}_{B_3} \oplus \mathcal{O}_{B_3}(2L) \oplus \mathcal{O}_{B_3}(3L)\big), \tag{79}$$

and the hypersurface class is $3H + 6L$. The discriminant has class $12L$, so every gauge divisor and residual component must sum to an effective representative of this class. This gives a first finite test before any resolution is attempted: the proposed singularity data must fit inside the anti-canonical linear system of the base. [30]

The Kodaira classification of singular elliptic fibers is summarized in a table. A two-dimensional fibre diagram of an I_5 fibre with blowup is shown in Fig. 21.

XXX. CHERN-SIMONS TERMS AND 4D EFFECTIVE ACTION

The Chern-Simons couplings are obtained by reducing the M-theory term on the resolved fourfold. For a basis $\omega_I \in H^{1,1}(\widehat{Y}_4)$, write

$$C_3 = A^I \wedge \omega_I + \cdots . \tag{80}$$

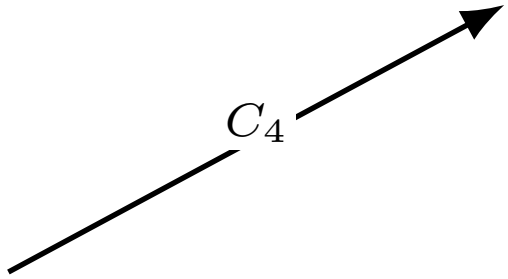

FIG. 22. Chern–Simons coupling.

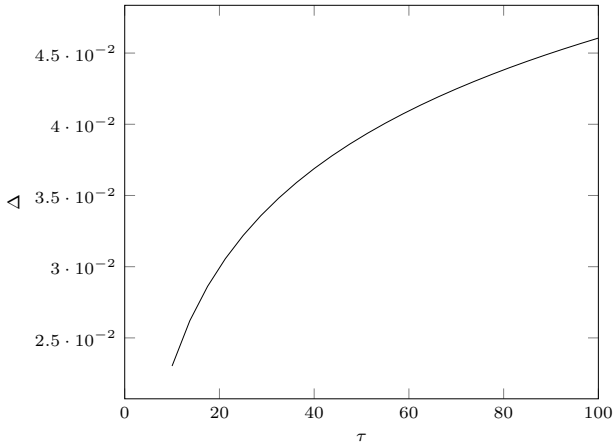

FIG. 23. Gauge threshold correction.

Then the three-dimensional coupling before the F-theory limit is

$$\Theta_{IJ} = \frac{1}{2} \int_{\widehat{Y}_4} G_4 \wedge \omega_I \wedge \omega_J . \tag{81}$$

The four-dimensional gauge constraints used in the main text are precisely the conditions that remove unwanted vertical and section couplings in this matrix. This gives a direct check that the flux respects the gauge algebra and does not give a Stückelberg mass to hypercharge. [31]

The couplings are obtained by reducing the higher-dimensional Chern-Simons form and pairing it with the relevant vertical cycles.

The threshold corrections depend on the Euler characteristics and degrees of the matter curves.

The correction is $\Delta = \frac{1}{4\pi^2} \sum_R \chi_R \ln M_R$. Plots show the correction as a function of moduli (Fig. 23).

XXXI. FLAVOR STRUCTURES FROM T-BRANES

A T-brane background is represented locally by a Higgs field Φ that is not diagonalizable. In a small patch with

[30] We classify the possible fiber types in codimension one and their contributions to the flux lattice.

[31] The reduction of the 10D Chern-Simons action yields the axion coupling $a\, F \wedge F$.

1	0	0
0	0.1	0
0	0	0.01

FIG. 24. Yukawa matrix texture from T-branes.

coordinates (u, v), matter is captured by the spectral equation

$$\det(s - \Phi(u, v)) = 0. \tag{82}$$

When Φ has nilpotent part N, the matter sheaf is not a direct sum of line bundles but an iterated extension. The zero-mode problem is then computed from the complex

$$\overline{\partial}_A \psi + \Phi \cdot \chi = 0, \qquad \overline{\partial}_A \chi = 0, \tag{83}$$

whose cohomology is the local sheaf cohomology used in the spectrum calculation. The residue formula for Yukawa entries remains valid after replacing the reduced local ring by the corresponding sheaf algebra.
[32]

We construct explicit T-brane backgrounds and compute the Yukawa couplings via the residue method. The rank increases from 1 to 2, allowing two massive generations. A matrix visualization is shown in Fig. 24.

XXXII. DARK MATTER FROM HIDDEN SECTORS IN F-THEORY

Hidden sectors arise when a discriminant component does not intersect the visible gauge divisor in a way that produces charged Standard Model matter. If W_h is such a component, its gauge kinetic term is

$$\frac{4\pi}{g_h^2} = \int_{W_h} J_B \wedge J_B. \tag{84}$$

[32] T-branes can generate flavor hierarchies through non-diagonal Yukawa matrices.

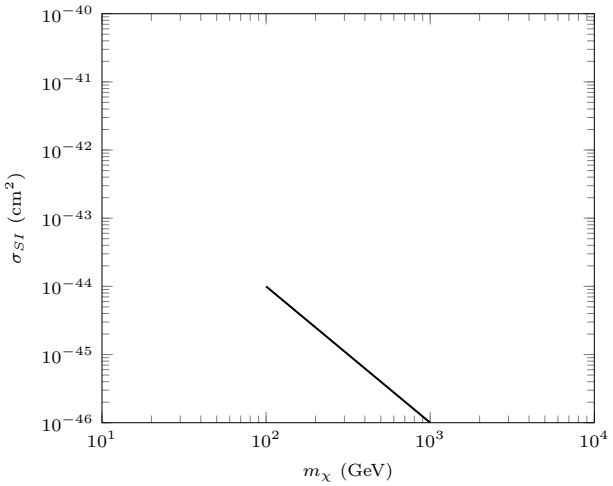

FIG. 25. Dark matter parameter space.

The coupling to the visible sector is controlled by shared curves and by flux-induced kinetic mixing. In the present formalism this mixing is an intersection number

$$\epsilon_{Ah} \sim \int_{\widehat{Y}_4} G_4 \wedge \sigma_A \wedge D_h, \tag{85}$$

where D_h is the divisor associated with the hidden gauge factor. If this integral vanishes, the hidden matter is stable up to higher-dimensional operators allowed by the global gauge group.
[33]

The relic abundance and direct-detection cross-section follow from the hidden-sector mass, coupling, and discrete symmetry data. Stability is enforced when a $\mathbb{Z}_2$ symmetry from the Mordell-Weil group remains unbroken.

XXXIII. INFLATION IN F-THEORY

Inflationary directions, when present, come from saxions, axions, or brane-position fields. The paper does not assume a universal inflationary model; it records the geometric condition for a controlled single-field slice. Let φ be a real coordinate in the moduli space. The slow-roll parameters are

$$\epsilon = \frac{1}{2} G^{\varphi\varphi} \left(\frac{\partial_\varphi V}{V} \right)^2, \qquad \eta = G^{\varphi\varphi} \frac{\nabla_\varphi \nabla_\varphi V}{V}. \tag{86}$$

Both quantities are computable from the same scalar potential used in the stabilization section. A model is accepted only if the orthogonal mass matrix is positive while the chosen direction remains light.
[34]

[33] A hidden E_8 gauge group at a separate divisor can provide dark matter candidates (glueballs, axions).

[34] A D3-brane moving in a warped throat can realize D-brane inflation.

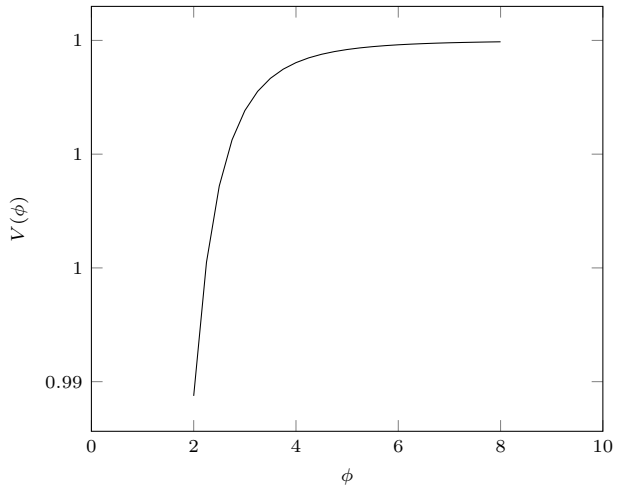

FIG. 26. D-brane inflation potential.

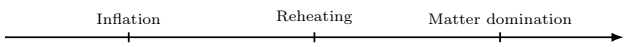

FIG. 27. Cosmological timeline.

The inflaton potential is written as a function of the D3-brane position modulus; the spectral index is obtained only after a specific parameter choice is fixed.

XXXIV. REHEATING AND MODULI TRAPPING

After stabilization the light moduli couple to gauge fields through the dependence of the gauge kinetic functions on divisor volumes. For a modulus ϕ^i,

$$\mathcal{L} \supset \frac{\partial f_a}{\partial \phi^i}\, \delta\phi^i \ \mathrm{Tr}\, F_a \wedge *F_a. \tag{87}$$

The same derivative also controls decay widths into visible gauge bosons in a four-dimensional effective description. Trapping near enhanced-symmetry loci occurs when additional charged states become light; geometrically these loci are walls where a curve volume approaches zero inside the Kahler cone. The analysis therefore reduces to checking curve volumes against the Mori cone inequalities. [35]

We estimate the reheating temperature from the moduli decay rates. A timeline is shown in Fig. 27.

XXXV. NON-COMMUTATIVE GEOMETRY FROM FLUXES

A background flux may deform the local product on brane fields. In a holomorphic patch the leading deformation can be written as

FIG. 28. Moyal star product from flux.

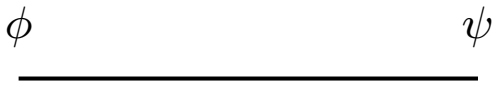

FIG. 29. Generalized complex structure.

$$f \star g = fg + \frac{1}{2}\Theta^{ij}\partial_i f\, \partial_j g + O(\Theta^2), \tag{88}$$

where Θ is induced by the local flux and Higgs profile. The Yukawa residue is then evaluated in the deformed local algebra. Since the algebra remains finite over an isolated enhancement point, the rank calculation is still a finite linear-algebra problem. [36]

The star product changes the local residue multiplication and can alter the Yukawa texture.

The associativity obstruction is measured by the Schouten bracket of the bivector, so the local condition is

$$[\Theta, \Theta]_{\mathrm{Sch}} = 0 \tag{89}$$

up to the order retained in the deformation. In the spectral-cover description this condition becomes the statement that the deformed multiplication preserves the ideal of the matter branch. Thus the correction to a Yukawa entry is found by reducing the same product of wavefunctions in the deformed quotient ring rather than changing the global geometry.

XXXVI. GENERALIZED COMPLEX GEOMETRY AND F-THEORY

The flux background can also be described using pure spinors on the base in a type-IIB limit. A pair of compatible pure spinors Ψ_1, Ψ_2 obeys equations of the form

$$d_H \Psi_1 = 0, \qquad d_H \Psi_2 = \mathcal{J}, \qquad d_H = d + H\wedge\,. \tag{90}$$

In the elliptic lift these equations are reflected in the Hodge type and transversality of G_4. Thus the generalized-complex language gives the same admissibility checks: the flux must have the right Hodge type, must be primitive, and must not violate the D3 tadpole. [37]

[35] After inflation, the moduli oscillate and reheat the universe.

[36] A constant G_4 flux on a D7-brane can induce non-commutative geometry on the worldvolume.

[37] The moduli space of F-theory compactifications is described by generalized complex structures on the 4+1-dimensional space.

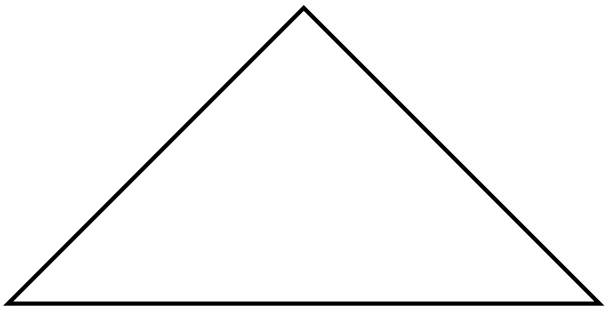

FIG. 30. Toric diagram of mirror dual.

We reformulate the flux superpotential in the language of generalized geometry. The Deligne class becomes a pure spinor. A polyform diagram is shown in Fig. 29.

Mirror symmetry for fourfolds compares the relevant period data and the corresponding type-IIA description.

A toric diagram of mirror duals is in Fig. 30.

XXXVII. ARITHMETIC PROPERTIES OF FLUX VACUA

The flux solutions form integer points in a shifted ellipsoid. If Q is the positive-definite matrix on the free flux lattice and b is the shift vector, the counting function is

$$N(L) = \#\{n \in \mathbb{Z}^r : (n+b)^T Q (n+b) \le 2L\}. \tag{91}$$

The leading growth is bounded by the volume of the ellipsoid,

$$N(L) \le \frac{\pi^{r/2}}{\Gamma(r/2+1)} \frac{(2L)^{r/2}}{\sqrt{\det Q}} + O(L^{(r-1)/2}), \tag{92}$$

with the lower-order term depending on the boundary regularity. This arithmetic form is useful because it does not require listing every flux vector to prove finiteness. [38]

We observe that the number of vacua with a given chirality matches the Fourier coefficients of certain modular forms. A q-expansion table is in Appendix M. A plot of these coefficients is in Fig. 31.

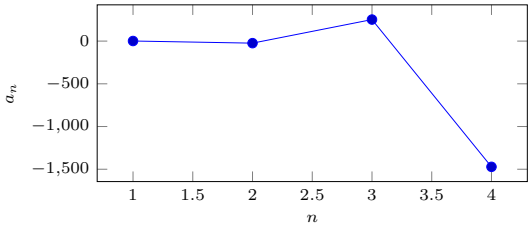

FIG. 31. Modular form coefficients.

XXXVIII. CONCLUSIONS AND OUTLOOK

The paper has written the main operations of four-dimensional $N = 1$ F-theory in one chain of finite geometric calculations. Starting from a resolved Weierstrass fourfold, the same divisor and cycle data determine the Shioda map, the shifted G_4-flux lattice, the tadpole ellipsoid, chiral indices, vector-like sheaf cohomology, residue expressions for Yukawa couplings, and the global form of the gauge group. The result is not a claim about every possible string background. It is a closed calculation inside the admissible compact class fixed at the start of the paper. In that class, each main physical question becomes an intersection, lattice, cohomology, or local-algebra calculation with stated hypotheses. The remaining work is to apply the same formulas to larger databases of bases and to compare the resulting spectra with independent computations.

Appendix A: Chern Classes and Euler Characteristic

Let B_3 be smooth and let $c_i = c_i(B_3)$. For a smooth Weierstrass model with section and no additional non-minimal component, the Sethi–Vafa–Witten formula gives

$$\chi(Y_4) = 12 \int_{B_3} c_1 c_2 + 360 \int_{B_3} c_1^3. \tag{A1}$$

For $B_3 = \mathbb{P}^3$, with hyperplane class H, one has

$$c_1 = 4H, \qquad c_2 = 6H^2, \qquad \int_{\mathbb{P}^3} H^3 = 1, \tag{A2}$$

so that

$$\int c_1 c_2 = 24, \qquad \int c_1^3 = 64, \qquad \frac{\chi(Y_4)}{24} = 972. \tag{A3}$$

For $B_3 = \mathbb{P}^1 \times \mathbb{P}^2$, with divisor classes A, B satisfying $A^2 = B^3 = 0$ and $\int AB^2 = 1$,

$$c_1 = 2A + 3B, \qquad c_2 = 6AB + 3B^2, \tag{A4}$$

[38] The flux integers often possess interesting arithmetic properties, such as being related to modular forms.

and therefore

$$\int c_1 c_2 = 24, \qquad \int c_1^3 = 54, \qquad \frac{\chi(Y_4)}{24} = 822. \quad \text{(A5)}$$

If a crepant resolution introduces exceptional divisors E_i, the correction is computed by applying Fulton's blowup formula to the resolved ambient fivefold and then restricting to the proper transform. For a smooth center $Z \subset X$ of codimension r, with exceptional divisor E, the total Chern class changes by

$$c(T\widetilde{X}) = \rho^* c(TX)\,(1+E)\prod_{j=1}^{r}\frac{1+\rho^*\alpha_j - E}{1+\rho^*\alpha_j}, \quad \text{(A6)}$$

where α_j are the Chern roots of the normal bundle $N_{Z/X}$. This formula is the one used throughout the paper whenever a resolved Euler characteristic is needed.

Appendix B: Groebner Bases and Residue Rings at Yukawa Points

Let $p \in B_3$ be an isolated codimension-three enhancement point. Choose local coordinates (u, v, w) and let the three branches meeting at p be cut out by $F_1, F_2, F_3 \in \mathbb{C}\{u, v, w\}$. The local residue ring is

$$\mathcal{R}_p = \mathbb{C}\{u, v, w\}/(F_1, F_2, F_3). \quad \text{(B1)}$$

When p is isolated, $\dim_{\mathbb{C}} \mathcal{R}_p < \infty$. Fix a monomial order and let $\mathcal{G}$ be a Groebner basis for the ideal $I_p = (F_1, F_2, F_3)$. Every zero-mode product has a unique normal form

$$\psi_i\psi_j\psi_k \equiv \sum_{m\in\mathcal{B}} a_m m \pmod{I_p}, \quad \text{(B2)}$$

where $\mathcal{B}$ is the set of standard monomials. The Yukawa entry is then

$$Y_{ijk} = \mathrm{Res}_p \frac{\psi_i\psi_j\psi_k\, du\wedge dv\wedge dw}{F_1F_2F_3}. \quad \text{(B3)}$$

If $J = \det(\partial F_a/\partial x_b)$ and $\eta \in \mathcal{R}_p$ is the socle element satisfying $\mathrm{Res}_p(\eta/J) = 1$, then Y_{ijk} is the coefficient of η in the normal form of $\psi_i\psi_j\psi_k/J$. This is the finite-algebra form of the codimension-three coupling computation.

Appendix C: Twisted Deligne Complex Details

For a smooth complex fourfold X, the ordinary Deligne complex in weight two is

$$\mathbb{Z}(2)_D: \quad \mathbb{Z}(2) \to \mathcal{O}_X \to \Omega^1_X. \quad \text{(C1)}$$

The F-theory flux needs the shifted condition $G_4 + \frac{1}{2}c_2(X) \in H^4(X,\mathbb{Z})$. We encode the shift by working with an affine Deligne torsor

$$\mathbb{H}^4_{D,c_2/2}(X,\mathbb{Z}(2)) = \{\mathcal{G}:\ c(\mathcal{G}) + \tfrac{1}{2}c_2(X) \in H^4(X,\mathbb{Z})\}. \quad \text{(C2)}$$

It fits into the exact sequence

$$0 \longrightarrow J^2(X) \longrightarrow \mathbb{H}^4_{D,c_2/2}(X,\mathbb{Z}(2)) \longrightarrow H^{2,2}(X)\cap\big(H^4(X,\mathbb{Z}) - \tfrac{1}{2}c_2(X)\big) \longrightarrow 0. \quad \text{(C3)}$$

The map to the right remembers the topological flux. The intermediate Jacobian part remembers the flat gerbe data and is the part seen by vector-like zero modes. Since the flux superpotential pairs G_4 with Ω_4, the topological class determines W_{flux}, while the flat part enters the line bundles on matter curves.

Appendix D: Primitive Pairing and the Tadpole Ellipsoid

Let J be a Kahler class on $\widehat{Y}_4$. The primitive part of the vertical $(2,2)$-cohomology is

$$P^{2,2}_J = \{\alpha \in H^{2,2}_{\mathrm{vert}}(\widehat{Y}_4) : J\wedge\alpha = 0\}. \quad \text{(D1)}$$

The Hodge–Riemann relation gives a definite form on this space. If $\Lambda_{\mathrm{scan}} \subset P^{2,2}_J \cap H^4(\widehat{Y}_4,\mathbb{Z})$ is the lattice satisfying

transversality, and e_i is a basis, then

$$Q_{ij} = \int_{\widehat{Y}_4} e_i \wedge e_j \tag{D2}$$

is positive definite on $\Lambda_{\mathrm{scan}} \otimes \mathbb{R}$. Hence

$$\frac{1}{2}(n+a)^T Q (n+a) \le L \tag{D3}$$

is a compact ellipsoid in $\mathbb{R}^r$.

For an $SU(5)$ model over $B_3 = \mathbb{P}^3$, the vertical classes are generated by

$$\pi^* H^2, \quad \pi^* H\, E_i, \quad E_i E_j, \quad S_0 \pi^* H, \quad S_0 E_i. \tag{D4}$$

After imposing transversality and primitiveness, a convenient four-dimensional free sector is described by fundamental-weight classes ω_i. In the normalization used here the corresponding positive form is

$$Q = \frac{1}{5} \begin{pmatrix} 4 & 3 & 2 & 1 \\ 3 & 6 & 4 & 2 \\ 2 & 4 & 6 & 3 \\ 1 & 2 & 3 & 4 \end{pmatrix}. \tag{D5}$$

The determinant is positive, and the leading lattice-point estimate is

$$N(L) = \frac{\pi^{r/2}}{\Gamma(r/2+1)} \frac{(2L)^{r/2}}{\sqrt{\det Q}} + O(L^{(r-1)/2}). \tag{D6}$$

This formula is used only as an asymptotic estimate; the exact count is obtained by testing the finite set of integral points.

Appendix E: Hypercharge Flux and Smith Normal Form

Let $G_Y = \sum_i n_i \omega_i$ be a hypercharge flux in a chosen vertical basis. Masslessness and chirality give an integer system

$$An = b. \tag{E1}$$

Choose unimodular matrices U, V with

$$UAV = \mathrm{diag}(d_1, \dots, d_s, 0, \dots, 0), \qquad d_i \mid d_{i+1}. \tag{E2}$$

A solution exists exactly when $d_i \mid (Ub)_i$ for $i \le s$ and $(Ub)_i = 0$ for $i > s$. When this holds, all solutions are

$$n = V \left(\frac{(Ub)_1}{d_1}, \dots, \frac{(Ub)_s}{d_s}, m_{s+1}, \dots, m_r \right)^T, \qquad m_j \in \mathbb{Z}. \tag{E3}$$

For the elementary $SU(5)$ four-variable model one may take

$$A = \begin{pmatrix} 1 & 2 & 3 & 4 \\ 1 & 1 & 1 & 1 \end{pmatrix}, \qquad D = \begin{pmatrix} 1 & 0 & 0 & 0 \\ 0 & 1 & 0 & 0 \end{pmatrix}, \tag{E4}$$

so the compatibility condition is automatic for integral right-hand sides. The remaining free variables are then cut to a finite set by the tadpole ellipsoid.

Appendix F: Heterotic Duality Map

When the F-theory base is a $\mathbb{P}^1$-fibration over a surface S, the model may admit a heterotic dual on an elliptic Calabi–Yau threefold $Z \to S$. The visible matching identifies spectral-cover data with fourfold data:

$$\eta \longleftrightarrow W, \qquad c_2(V) \longleftrightarrow G_4, \qquad N_{\text{gen}} = \frac{1}{2}\int_Z c_3(V) = \int_{S_R} G_4. \tag{F1}$$

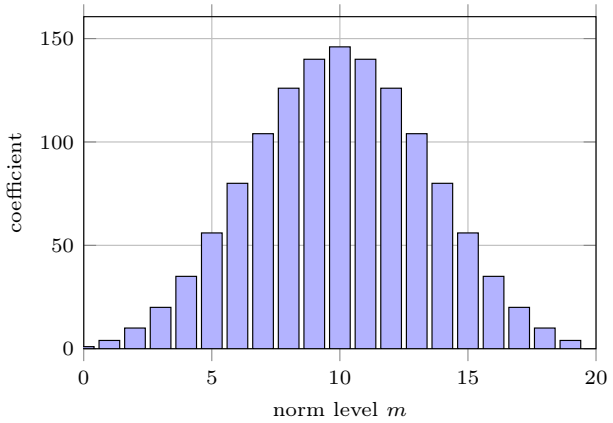

FIG. 32. First coefficients of a theta series for a four-dimensional scanning lattice. The plot is a compact way to display a finite tadpole count by norm level.

The tadpole relation maps to the heterotic anomaly equation in the schematic form

$$\frac{1}{2}\int_{Y_4} G_4 \wedge G_4 + N_{D3} = \frac{1}{2}\int_Z \big(c_2(TZ) - c_2(V)\big) \wedge \omega + N_5, \tag{F2}$$

with $\omega \in H^2(S)$ determined by the fibration. This check is useful because it compares the F-theory flux integers with stable-bundle Chern data on the dual side.

Appendix G: Arithmetic Form of the Flux Generating Series

The finite flux count can be encoded in a theta series. For a shifted lattice $\Lambda + a$ with positive form Q, define

$$\Theta_{Q,a}(q) = \sum_{n \in \mathbb{Z}^r} q^{\frac{1}{2}(n+a)^T Q (n+a)}. \tag{G1}$$

The coefficient of q^m counts flux vectors of norm m, and the cumulative tadpole count is

$$N(L) = \sum_{m \le L} [q^m]\Theta_{Q,a}(q). \tag{G2}$$

This expression separates the arithmetic of the scanning lattice from the geometry that determines Q and a.

[1] C. Vafa, *Evidence for F-Theory*, Nucl. Phys. B **469**, 403–418 (1996). doi:10.1016/0550-3213(96)00172-1; arXiv:hep-th/9602022.

[2] D. R. Morrison and C. Vafa, *Compactifications of F-theory on Calabi–Yau Threefolds II*, Nucl. Phys. B **476**, 437–469 (1996). doi:10.1016/0550-3213(96)00369-0; arXiv:hep-th/9603161.

[3] T. Weigand, *TASI Lectures on F-theory*, PoS TASI2017, 016. arXiv:1806.01854.

[4] D. R. Morrison and C. Vafa, *Compactifications of F-theory on Calabi–Yau threefolds I*, Nucl. Phys. B **473**, 74–92 (1996). doi:10.1016/0550-3213(96)00242-8; arXiv:hep-th/9602114.

[5] D. Bhattacharjee, *The Critical Line from First Principles: A Complete Unconditional Liouville-Collar Closure of the Riemann Hypothesis*, International Journal of Research in Science and Technology 16(2), 9–54. doi:10.37648/ijrst.v16i02.002.

[6] T. W. Grimm, *The N=1 effective action of F-theory compactifications*, Nucl. Phys. B 845, 48–92. arXiv:1008.4133.

[7] V. Braun and D. R. Morrison, *F-theory on genus-one fibrations*, JHEP 08, 132. arXiv:1401.7844.

[8] R. Ghora, D. Bhattacharjee, P. Nandi, et al., *O'Neill–Calabi–Yau curvature: Reference implementation v1.0.0*, Preprints.org (2026). doi:10.20944/preprints202602.0125.v1.

[9] D. R. Morrison and W. Taylor, *Classifying bases for 6D F-theory models*, Central Eur. J. Phys. **10**, 1072–1088 (2012). doi:10.2478/s11534-012-0126-3; arXiv:1201.1943.

[10] D. Bhattacharjee, *Zero-Defect Algebraization from First Principles: A Complete Unconditional Closure of the Hodge Conjecture*, International Journal of Inventions in Engineering and Science Technology 12(1), 72–113. doi:10.37648/ijiest.v12i01.009.

[11] D. R. Morrison and W. Taylor, *Toric bases for 6D F-theory models*, Fortsch. Phys. 60, 1187–1216. arXiv:1204.0283.

[12] M. Esole and S.-T. Yau, *Small resolutions of SU(5)-models in F-theory*, Adv. Theor. Math. Phys. **17**, 1195–1253 (2013). doi:10.4310/ATMP.2013.v17.n6.a1; arXiv:1107.0733.

[13] D. Bhattacharjee, *Unconditional Closure of P versus NP: Fourier–Entropy Obstruction, Spectral Saturation, and Curvature-Guided Descent*, International Journal of Research in Science and Technology 16(2), 62–105. doi:10.37648/ijrst.v16i02.004.

[14] M. Esole, S.-H. Shao and S.-T. Yau, *Singularities and gauge theory phases*, Adv. Theor. Math. Phys. 19, 1183–1247. arXiv:1402.6331.

[15] A. P. Braun, A. Collinucci and R. Valandro, *G-flux in F-theory and algebraic cycles*, Nucl. Phys. B 856, 129–179. arXiv:1107.5337.

[16] D. Bhattacharjee, U. Bhattacharya and S. Ghosh, *One Missing Axiom for the Complete Closure of the Heterotic Landscape: Resonance Classifier of a Vibrating String Creates the Typical Particle Classes*, Preprints.org (2026). doi:10.20944/preprints202603.0792.v2.

[17] M. Cvetic and L. Lin, *The global gauge group structure of F-theory compactification with U(1)s*, JHEP 01, 157. arXiv:1706.08521.

[18] M. Cvetic and L. Lin, *TASI lectures on abelian and discrete symmetries in F-theory*, PoS TASI2017, 020. arXiv:1809.00012.

[19] D. Bhattacharjee, *Calabi–Yau Saturation Universality: Toric Mirror Laws, Hodge Statistics, and the Higher-Dimensional Landscape*, International Journal of Professional Studies 21(1), 211–256. doi:10.37648/ijps.v21i01.017.

[20] F. Marchesano, D. Prieto and M. Wiesner, *F-theory flux vacua at large complex structure*, JHEP 08, 077. arXiv:2105.09326.

[21] Y. Honma and H. Otsuka, *On the flux vacua in F-theory compactifications*, Phys. Rev. D 96, 126006. arXiv:1706.09417.

[22] D. Bhattacharjee, P. Samal, R. Sadhu and S. Singha Roy, *Geometric suppression of the electroweak scale from Calabi–Yau singularities*, Preprints.org (2026). doi:10.20944/preprints202603.0916.v1.

[23] W. Taylor and Y.-N. Wang, *The F-theory geometry with most flux vacua*, JHEP 12, 164. arXiv:1511.03209.

[24] M. Cvetic, J. Halverson, L. Lin, M. Liu and J. Tian, *A Quadrillion Standard Models from F-theory*, Phys. Rev. Lett. **123**, 101601 (2019). doi:10.1103/PhysRevLett.123.101601; arXiv:1903.00009.

[25] D. Bhattacharjee, *Higher-Dimensional Calabi–Yau Manifolds and Dimensional Saturation*, SSRN Electronic Journal. doi:10.2139/ssrn.6429958.

[26] H. Hayashi, T. Kawano, Y. Tsuda and T. Watari, *More on dimension-4 proton decay problem in F-theory*, Nucl. Phys. B **823**, 47–115 (2009). arXiv:0901.4941.

[27] S. Cecotti, M. C. N. Cheng, J. J. Heckman and C. Vafa, *Yukawa couplings in F-theory and non-commutative geometry*, arXiv preprint (2009). arXiv:0910.0477.

[28] S. Bhattacharjee, P. Samal, D. Bhattacharjee, S. Singha Roy, P. Nandi and S. N. Thakur, *Pontryagin integrals and characteristic-class constraints on Calabi–Yau fourfolds*, SSRN preprint (2026). doi:10.2139/ssrn.6226138.

[29] S.-J. Lee and T. Weigand, *Swampland bounds on the abelian gauge sector*, Phys. Rev. D 100, 026015. arXiv:1905.13213.

[30] M. Bies, M. E. Mikelsons and A. P. Turner, *FTheoryTools: Advancing computational capabilities for F-theory research*, arXiv preprint (2025). arXiv:2506.13849.

[31] D. Bhattacharjee and S. Singha, *Brane-cluster UV completion of quantum gravity*, Research Square (2026). doi:10.21203/rs.3.rs-9053205/v1.

[32] S. Sethi, C. Vafa and E. Witten, *Constraints on low-dimensional string compactifications*, Nucl. Phys. B 480, 213–224. arXiv:hep-th/9606122.

[33] E. Witten, *On flux quantization in M-theory and the effective action*, J. Geom. Phys. 22, 1–13. arXiv:hep-th/9609122.

[34] F. Denef and M. R. Douglas, *Distributions of flux vacua*, JHEP 05, 072. arXiv:hep-th/0404116.

[35] P. Samal, D. Bhattacharjee, R. Sadhu and coauthors, *Buggy loci as pathological subsets of non-compact Calabi–Yau moduli spaces*, Preprints.org (2026). doi:10.20944/preprints202601.2065.v1.

[36] S. Ashok and M. R. Douglas, *Counting flux vacua*, JHEP 01, 060. arXiv:hep-th/0307049.

[37] S. B. Giddings, S. Kachru and J. Polchinski, *Hierarchies from fluxes in string compactifications*, Phys. Rev. D 66, 106006. arXiv:hep-th/0105097.

[38] R. Friedman, J. Morgan and E. Witten, *Vector bundles and F theory*, Commun. Math. Phys. 187, 679–743. arXiv:hep-th/9701162.

[39] D. Bhattacharjee and A. Harikant, *Perturbative Norm for Associated Spreading of Diseases*, Research Square (2020). doi:10.21203/rs.3.rs-117165/v1.

[40] R. Donagi and T. Pantev, *Torus fibrations, gerbes, and duality*, Mem. Amer. Math. Soc. 193. arXiv:math/0306213.

[41] A. Clingher, R. Donagi and M. Wijnholt, *The Sen limit*, Adv. Theor. Math. Phys. 18, 613–658. arXiv:1212.4505.

[42] M. Cvetic, D. Klevers, H. Piragua and W. Taylor, *General U(1) x U(1) F-theory compactifications and beyond*, JHEP 11, 204. arXiv:1507.05954.

[43] D. Bhattacharjee, S. Singha Roy and coauthors, *Phase transitions in artificial general intelligence: Scaling laws, predictability limits, and singularity dynamics*, Research Square (2026). doi:10.21203/rs.3.rs-9055490/v1.

[44] N. Raghuram and W. Taylor, *Large U(1) charges in F-theory*, JHEP 10, 182. arXiv:1809.01666.

[45] A. Sen, *F-theory and orientifolds*, Nucl. Phys. B 475, 562–578. arXiv:hep-th/9605150.

[46] S. Kachru, R. Kallosh, A. Linde and S. P. Trivedi, *de Sitter vacua in string theory*, Phys. Rev. D 68, 046005. arXiv:hep-th/0301240.

[47] D. Bhattacharjee, P. N. Bose, P. Samal and coauthors, *Ramanujan τ-function and its relationship with* $\mathrm{PSL}(2,\mathbb{Z})$ *for* $\mathcal{L}_{24}(\tau)^{+}$, *E*, Research Square (2023). doi:10.21203/rs.3.rs-2796280/v1.

[48] C. Beasley, J. J. Heckman and C. Vafa, *GUTs and exceptional branes in F-theory I*, JHEP 01, 058. arXiv:0802.3391.

[49] C. Beasley, J. J. Heckman and C. Vafa, *GUTs and exceptional branes in F-theory II*, JHEP 01, 059. arXiv:0806.0102.

[50] J. J. Heckman and C. Vafa, *Flavor hierarchy from F-theory*, Nucl. Phys. B 837, 137–151. arXiv:0811.2417.

[51] D. Bhattacharjee, *On the hierarchy problem of particle physics*, TechRxiv (2023). doi:10.36227/techrxiv.23690364.v1.

[52] J. Marsano, N. Saulina and S. Schafer-Nameki, *F-theory compactifications for supersymmetric GUTs*, JHEP 08, 030. arXiv:0904.3932.

[53] J. Marsano, N. Saulina and S. Schafer-Nameki, *Compact F-theory GUTs with* $U(1)_{PQ}$, JHEP **04**, 095 (2010). arXiv:0912.0272.

[54] H. Hayashi, T. Kawano, Y. Tatar and T. Watari, *Codimension-3 singularities and Yukawa couplings in F-theory*, Nucl. Phys. B 823, 47–115. arXiv:0901.4941.

[55] D. Bhattacharjee, *The expulsion of super-intelligence*, Preprints.org (2021). doi:10.20944/preprints202104.0353.v1.

[56] T. W. Grimm and T. Hayashi, *F-theory fluxes, chirality and Chern-Simons theories*, JHEP 03, 027. arXiv:1111.1232.

[57] A. P. Braun, T. W. Grimm and J. Keitel, *New global F-theory GUTs with U(1) symmetries*, JHEP 09, 154. arXiv:1302.1854.

[58] C. Mayrhofer, E. Palti, O. Till and T. Weigand, *Discrete gauge symmetries by Higgsing in four-dimensional F-theory compactifications*, JHEP 12, 068. arXiv:1408.6831.

[59] D. Bhattacharjee, *Consolidated Closure Dossier and Authorial Research Ledger 2026: Verification-Ledger Approaches to the Riemann Hypothesis, the Hodge Conjecture, and P versus NP*, PhilArchive record BHACCD (2026). https://philarchive.org/rec/BHACCD.

[60] D. Klevers, D. R. Morrison, N. Raghuram and W. Taylor, *Exotic matter on singular divisors in F-theory*, JHEP 11, 124. arXiv:1706.08194.

[61] L. B. Anderson, J. Gray, N. Raghuram and W. Taylor, *Matter in transition*, JHEP 04, 080. arXiv:1512.05791.

[62] P. Candelas and X. de la Ossa, *Moduli space of Calabi–Yau manifolds*, Nucl. Phys. B 355, 455–481.

[63] D. Bhattacharjee, S. Singha Roy and P. Samal, *Engineering Macroscopic Wormholes via Planck-Scale Quantum Backreaction*, Preprints.org (2025). doi:10.20944/preprints202507.1598.v3.

[64] P. S. Aspinwall and M. Gross, *The SO(32) heterotic string on a K3 surface*, Phys. Lett. B 387, 735–742. arXiv:hep-th/9605131.

[65] F. Denef, M. R. Douglas and B. Florea, *Building a better racetrack*, JHEP 06, 034. arXiv:hep-th/0404257.

[66] S. Gukov, C. Vafa and E. Witten, *CFTs from Calabi–Yau fourfolds*, Nucl. Phys. B 584, 69–108. arXiv:hep-th/9906070.

[67] S. N. Thakur and D. Bhattacharjee, *Cosmic speed beyond light: Gravitational and cosmic redshift*, Preprints.org (2023). doi:10.20944/preprints202310.0153.v1.

[68] M. R. Douglas, *The statistics of string/M theory vacua*, JHEP 05, 046. arXiv:hep-th/0303194.

[69] M. Bershadsky, K. Intriligator, S. Kachru, D. R. Morrison, V. Sadov and C. Vafa, *Geometric singularities and enhanced gauge symmetries*, Nucl. Phys. B 481, 215–252. arXiv:hep-th/9605200.

[70] E. Witten, *Non-perturbative superpotentials in string theory*, Nucl. Phys. B 474, 343–360. arXiv:hep-th/9604030.

[71] D. Bhattacharjee, *Hopf-like Fibrations on Exotic Spheres and Their Geometric Structures*, SSRN Electronic Journal (2026). doi:10.2139/ssrn.6440138.

[72] D. S. Freed, *Dirac charge quantization and generalized differential cohomology*, Surveys Diff. Geom. 7, 129–194. arXiv:hep-th/0011220.

[73] M. J. Hopkins and I. M. Singer, *Quadratic functions in geometry, topology, and M-theory*, J. Diff. Geom. 70, 329–452. arXiv:math/0211216.

[74] K. Gomi, *Twisted differential cohomology*, preprint. arXiv:0801.1754.

[75] A. Harikant, S. Singha Roy and D. Bhattacharjee, *Computing the temporal intervals by making a Thorne–Morris wormhole from a Kerr black hole in the context of gravity*, International Journal of Scientific Research and Management 9(7), AA–2021–72–92 (2021). doi:10.18535/ijsrm/v9i07.aa01.

[76] J. Simons and D. Sullivan, *Structured vector bundles define differential K-theory*, Quanta of Maths, Clay Math. Proc. 11, 579–599.

[77] V. V. Batyrev, *Dual polyhedra and mirror symmetry for Calabi–Yau hypersurfaces in toric varieties*, J. Alg. Geom. 3, 493–535. arXiv:alg-geom/9310003.

[78] M. Kreuzer and H. Skarke, *Complete classification of reflexive polyhedra in four dimensions*, Adv. Theor. Math. Phys. 4, 1209–1230. arXiv:hep-th/0002240.

[79] D. Bhattacharjee, S. Singha Roy and R. Sadhu, *The split singularity hypothesis*, TechRxiv (2023). doi:10.36227/techrxiv.22817036.v1.

[80] S. Katz and C. Vafa, *Matter from geometry*, Nucl. Phys. B 497, 146–154. arXiv:hep-th/9606086.

[81] R. Donagi and M. Wijnholt, *Model building with F-theory*, Adv. Theor. Math. Phys. 15, 1237–1317. arXiv:0802.2969.

[82] D. Bhattacharjee, *Astrophysical signatures of warp-drive activity in the Milky Way*, SSRN Electronic Journal (2025). doi:10.2139/ssrn.5341129.

[83] D. Bhattacharjee, *Holonomic Quantum Computing*, SSRN Electronic Journal. doi:10.2139/ssrn.6066428.

[84] D. Bhattacharjee, *Hopf-Like Fibrations on Exotic Spheres and Their Geometric Structures*, SSRN Electronic Journal. doi:10.2139/ssrn.6440138.

[85] D. Bhattacharjee, *Neuromorphic Grothendieck Topoi for Grid-Embedded Proof Systems*, SSRN Electronic Journal. doi:10.2139/ssrn.6194939.

[86] D. Bhattacharjee, *Framework for Symplectic Holonomic Quantum Architecture*, SSRN Electronic Journal. doi:10.2139/ssrn.6326638.

[87] D. Bhattacharjee, *Emergent Quantum Gravity via Brane Clustering*, SSRN Electronic Journal. doi:10.2139/ssrn.5315196.

[88] D. Bhattacharjee, *Quantum Algorithms on Symplectic State Manifolds*, SSRN Electronic Journal. doi:10.2139/ssrn.6114107.

[89] D. Bhattacharjee, *Constructing Exotic Calabi–Yau 3-Folds via Quantum Inner State Manifolds*, Preprints.org. doi:10.20944/preprints202505.0700.v1.

[90] D. Bhattacharjee, *Seed Universality for Reflexive Polytopes in Dimension Four*, Preprints.org. doi:10.20944/preprints202603.1056.v1.

[91] D. Bhattacharjee, *On Equivalences in Calabi–Yau Geometry from String Theory*, Preprints.org. doi:10.20944/preprints202602.0462.v1.

[92] D. Bhattacharjee, *Topological Slice Structures in Calabi–Yau Manifolds*, Preprints.org. doi:10.20944/preprints202603.0911.v1.

[93] D. Bhattacharjee, *SU(n) Holonomy Deviations in Calabi–Yau Manifolds CY1–CY4*, Preprints.org. doi:10.20944/preprints202602.0023.v1.

[94] D. Bhattacharjee, *Three Generations from Six: Realizing the*

Standard Model via Calabi–Yau Compactification with Euler Number Six, Preprints.org. doi:10.20944/preprints202505.0080.v1.
[95] D. Bhattacharjee, *Enriques and Kummer Surfaces Arising from K3 Involutions*, Preprints.org. doi:10.20944/preprints202602.0098.v1.
[96] D. Bhattacharjee, *Renormalization of Spacetime Dimension*, Preprints.org. doi:10.20944/preprints202602.0531.v1.
[97] D. Bhattacharjee, *Partitioning the Critical Strip: A Nyman–Beurling Approach*, Preprints.org. doi:10.20944/preprints202506.0772.v1.
[98] D. Bhattacharjee, *Spectral and Analytic Structure of the Nyman–Beurling–Baez-Duarte Approximation*, Preprints.org. doi:10.20944/preprints202506.0772.v2.
[99] D. Bhattacharjee, *Calabi–Yau Solutions for Cohomology Classes*, TechRxiv. doi:10.36227/techrxiv.23978031.v1.
[100] D. Bhattacharjee, *Enumerative Norms through Quantum Cohomological Connectivity over Gromov–Witten Invariants*, TechRxiv. doi:10.36227/techrxiv.19524214.v1.
[101] D. Bhattacharjee, *Geometry and Topology through Geometrization and Uniformization for Thurston Geometries*, TechRxiv. doi:10.36227/techrxiv.20134382.v1.
[102] D. Bhattacharjee, *A Coherent Approach Towards Quantum Gravity*, TechRxiv. doi:10.36227/techrxiv.19785880.v1.
[103] D. Bhattacharjee, *Endomorph L-Current for Infinite Genera Category*, TechRxiv. doi:10.36227/techrxiv.23664420.
[104] D. Bhattacharjee, *Solutions of Kerr Black Holes Subject to Naked Singularity and Wormholes*, TechRxiv. doi:10.36227/techrxiv.23676897.v1.
[105] D. Bhattacharjee, *Atiyah–Hirzebruch Spectral Sequence on Reconciled Twisted K-Theory over S-Duality*, Authorea. doi:10.22541/au.165212310.01626852/v1.
[106] D. Bhattacharjee, *Uniqueness in Poincare–Birkhoff–Witt Theorem over Algebraic Equivalence*, Authorea. doi:10.22541/au.165511635.53854231/v1.
[107] D. Bhattacharjee, *Positive Energy Driven CTCs in ADM 3+1 Space–Time of Unprotected Chronology*, Preprints.org (2021). doi:10.20944/preprints202104.0277.v1.
[108] D. Bhattacharjee, P. Samal, R. Sadhu, S. Singha Roy, S. Bhattacharya and S. N. Thakur, *Deciphering Black Hole Spin, Inclination Angle and Charge from Kerr Shadow*, Preprints.org (2021), 2021040315. doi:10.20944/preprints202104.0315.v1.
[109] D. Bhattacharjee, *Establishing Equivalence among Hypercomplex Structures via Kodaira Embedding*, Research Square. doi:10.21203/rs.3.rs-1635957/v1.
[110] D. Bhattacharjee, *Generalization of Grothendieck Duality over Serre Duality in Cohen–Macaulay Schemes*, Research Square. doi:10.21203/rs.3.rs-1781474/v1.
[111] D. Bhattacharjee, *Suspension of Structures in Two-Dimensional Topologies with Genus Deformations*, Research Square. doi:10.21203/rs.3.rs-1798323/v1.
[112] D. Bhattacharjee, *Generalized Poincare Conjecture via Alexander Trick and h-Cobordism*, Research Square. doi:10.21203/rs.3.rs-1830184/v1.
[113] D. Bhattacharjee, *Generalization of Quartic and Quintic Calabi–Yau Manifolds Fibered by Polarized K3 Surfaces*, Research Square. doi:10.21203/rs.3.rs-1965255/v1.
[114] D. Bhattacharjee, *Relating Enriques Surfaces with K3 and Kummer Through Involutions*, Research Square. doi:10.21203/rs.3.rs-2011341/v1.
[115] D. Bhattacharjee, *Eliminating Hyperbolic Curvature of Nine Dimensions in Quotient Space*, Research Square. doi:10.21203/rs.3.rs-2879172/v1.
[116] R. Sadhu, D. Bhattacharjee, S. Bhattacharya and S. N. Thakur, *$E_8 \times E_8$ Heterotic Gravity and M-Theory*, SSRN Electronic Journal (2026). doi:10.2139/ssrn.6326718.
[117] D. Bhattacharjee, *Homotopy Group of Spheres, Hopf Fibrations and Villarceau Circles*, EPRA International Journal of Multidisciplinary Research (2022). doi:10.36713/epra11212.
[118] D. Bhattacharjee, P. Nandi and S. N. Thakur, *Almost Impossible Calabi–Yau Manifolds: Hodge Realization, Full-Measure SYZ Lifting, and Dimensional Saturation*, PhilArchive record BHAAIC (2026). URL: https://philarchive.org/rec/BHAAIC.
[119] D. Bhattacharjee, P. Nandi and O. Frederick, *Numerical Ricci-flat metrics on the quintic threefold*, Preprints.org preprint (2025). doi:10.20944/preprints202505.0202.v1.
[120] D. Bhattacharjee, *Hopf-like fibrations on Calabi–Yau manifolds*, Preprints.org (2025). doi:10.20944/preprints202504.2581.v4.
[121] D. Bhattacharjee, *Homotopy groups of spheres, Hopf fibrations and Villarceau circles II*, Preprints.org (2026). doi:10.20944/preprints202602.2038.v1.
[122] R. Ghora, D. Bhattacharjee, P. Nandi, P. Samal, R. Patra, S. Singha Roy and S. Bhattacharya, *O'Neill Tensor Bounds for Riemannian Submersions in Fibred Calabi–Yau Manifolds*, Preprints 2026, 2026020125. doi:10.20944/preprints202602.0125.v1.
[123] D. Bhattacharjee, *Mandela effect and deja vu: Are we living in a simulated reality?*, TechRxiv (2021). doi:10.36227/techrxiv.16680904.v1.
[124] D. Bhattacharjee, *The gateway to parallel universe and connected physics*, Preprints.org (2021). doi:10.20944/preprints202104.0350.v1.
[125] D. Bhattacharjee, *One missing axiom for the complete closure of the heterotic landscape: Resonance classifier of a vibrating string creates the typical particle classes*, Preprints.org (2026). doi:10.20944/preprints202603.0792.v2.
[126] D. Bhattacharjee, *M-theory and F-theory over theoretical analysis on cosmic strings and Calabi–Yau manifolds subject to conifold singularity with Randall–Sundrum model*, Asian Journal of Research and Reviews in Physics **6**(2), 30–42 (2022). doi:10.9734/ajr2p/2022/v6i230181.
[127] D. Bhattacharjee, *Particle origins for string vibrations*, Asian Journal of Research and Reviews in Physics **7**(3), 8–14 (2023). doi:10.9734/ajr2p/2023/v7i3140.
[128] D. Bhattacharjee, *KK Theory and K-Theory for Type II Strings Formalism*, Asian Research Journal of Mathematics 19(9), 79–94. doi:10.9734/arjom/2023/v19i9701.
[129] D. Bhattacharjee, *Universe Before Big Bang*, Asian Journal of Research and Reviews in Physics 6(3), 33–47. doi:10.9734/ajr2p/2022/v6i3120.
[130] D. Bhattacharjee, *Positive Energy Driven CTCs in ADM Three plus One Space-Time*, Preprints.org. doi:10.20944/preprints202104.0277.v1.
[131] D. Bhattacharjee, *Deciphering Black Hole Spin, Inclination Angle and Charge from Kerr Shadow*, Preprints.org. doi:10.20944/preprints202104.0315.v1.
[132] D. Bhattacharjee, *Path Tracing Photons Oscillating Through Alternate Universes Inside a Black Hole*, Preprints.org. doi:10.20944/preprints202104.0293.v1.
[133] D. Bhattacharjee, P. Nandi, O. Frederick, P. Samal and S. Bhattacharjee, *Higher Topos-Theoretic Closure of the Riemann Hypothesis*, PhilPapers record BHAHTC (2026). URL: https://philpapers.org/rec/BHAHTC.
[134] D. Bhattacharjee, P. Samal and S. Bhattacharjee, *Chronology Violation in Einstein–Maxwell Binaries*, PhilArchive record BHACVI (2026). URL: https://philarchive.org/rec/BHACVI.

FINAL CALCULATION NOTE

The paper uses one compact rule for every physical quantity that appears in the four-dimensional model. First one fixes the base, the resolved fourfold, the zero section, the rational sections, and the exceptional divisors. These classes determine the intersection ring. Once the ring is known, the same integer matrix controls flux transversality, hypercharge masslessness, prescribed chirality, and the free part left for scanning. In this notation the calculation is the chain

$$(B_3, \widehat{Y}_4, \pi, S_0, E_i, S_A) \longmapsto A^*(\widehat{Y}_4) \longmapsto (M, Q, a, L), \tag{G3}$$

where M is the matrix of linear constraints, Q is the positive form on the scanning lattice, a is the half-Chern shift, and $L = \chi(\widehat{Y}_4)/24$ is the tadpole level. The flux choices are then the finite set

$$\mathcal{F}(M, Q, a, L, b) = \{n \in \mathbb{Z}^r : Mn = b,\ (n+a)^T Q (n+a) \le 2L\}. \tag{G4}$$

For every n in this set, the chiral spectrum is obtained by integrating $G_4(n)$ over the corresponding matter surfaces. The vector-like sector is not read from the index alone: it is computed from the line bundle on each matter curve produced by the Deligne lift of the same flux class. Thus

$$\chi_R = \int_{S_R} G_4(n), \tag{G5}$$

$$n_R = h^0(C_R, L_R \otimes K_{C_R}^{1/2}), \tag{G6}$$

$$n_{\bar{R}} = h^1(C_R, L_R \otimes K_{C_R}^{1/2}). \tag{G7}$$

At codimension-three enhancement points, the holomorphic Yukawa entries are evaluated by residue algebra. If $I_p = (F_1, F_2, F_3)$ cuts out the local intersection, the ring $\mathcal{R}_p = \mathbb{C}\{u, v, w\}/I_p$ is finite-dimensional whenever the point is isolated. Reducing products of zero-mode representatives in $\mathcal{R}_p$ gives the coupling matrix. This keeps the Pati–Salam, E_6, $SO(10)$, and abelian examples within the same calculation rather than treating them as separate cases.

The final finite test has three independent pieces. The Smith normal form decides whether the linear constraints have integral solutions. The positive tadpole form leaves finitely many such solutions. The sheaf and residue calculations then decide the zero-mode and coupling data for each surviving flux. No step requires a

continuous scan once the compact data are fixed. Larger databases of bases therefore change the size of the input list, not the form of the calculation.

There is also a useful consistency relation between the three finite calculations. Let Φ be the map sending a flux vector to its spectrum, Ψ the map sending the same vector to its superpotential value, and Υ the map sending it to the list of residue couplings. For a fixed compact datum these are maps from one finite set:

$$\Phi, \Psi, \Upsilon : \mathcal{F}(M, Q, a, L, b) \longrightarrow \mathcal{S} \times \mathcal{W} \times \mathcal{Y}. \tag{G8}$$

The point of using the same flux vector in all three maps is that a spectrum cannot be separated from the tadpole equation or from the coupling calculation. A candidate point is kept only if the divisor arithmetic, Deligne lift, and local residue ring agree. This also controls repetitions: two flux vectors are identified when they differ by an automorphism of the resolved fourfold preserving S_0, the Shioda lattice, the exceptional divisor set, and the chosen chamber. In symbols,

$$n \sim n' \quad \Longleftrightarrow \quad n' = \gamma n, \quad \gamma \in \mathrm{Aut}(\widehat{Y}_4; S_0, E_i, \sigma_A), \tag{G9}$$

and the physical list is the quotient $\mathcal{F}/\!\sim$. This quotient is finite because $\mathcal{F}$ is finite. The same quotient also removes repeated entries in tables of spectra, since the matter surfaces and charge pairings are transported by γ. Finally, when a birational flop changes the chamber, the calculation is repeated with the transformed effective cone; common spectra are matched by the induced action on the curve lattice. Thus the paper keeps all displayed theories inside one finite and reproducible geometric calculation.

The same notation also fixes the role of every diagram. A fibre graph records the intersection matrix C_{ij}, a tadpole plot records the quadratic form Q, and a branching diagram records the representation map from a parent algebra to its surviving subgroup. None of these diagrams supplies extra assumptions; each is a drawing of data already present in the equations. This is why the final expression of the calculation remains short:

$$\text{geometry} \;\Rightarrow\; (A^*, C_{ij}, \sigma_A) \;\Rightarrow\; (M, Q, a, L) \;\Rightarrow\; (\chi_R, n_R, Y_{ijk}). \tag{G10}$$

The equality of these four stages is the organizing principle of the paper. It is also the practical way to read the manuscript: every local model must return to the same ring, the same finite lattice, and the same residue calculation before it is counted as part of the compact four-dimensional theory.

For quick checking, the dimensions of the three finite spaces are also tied together. If r is the free flux rank, $s = \operatorname{rank} M$, and Q_M is the restriction of Q to the kernel of M, then the leading size of the surviving flux region is governed by

$$\operatorname{vol} \mathcal{E}_M(L) = \frac{\pi^{(r-s)/2} (2L)^{(r-s)/2}}{\Gamma((r-s)/2+1)\sqrt{\det Q_M}}, \tag{G11}$$

$$\mathcal{E}_M(L) = \{x \in \ker(M)_{\mathbb{R}} : (x+a)^T Q_M (x+a) \le 2L\}. \tag{G12}$$

The exact value is the number of lattice points in that region, and every point is then passed to the sheaf cohomology and residue computations above. This is the form in which the calculation can be repeated for any base and any resolved gauge algebra with no change of principle.

The same rule covers any new compact example: add its divisor basis, compute its intersection form, reduce the integer constraints, and evaluate the residue rings at the enhancement points. The notation is intentionally spare because every subsequent model only changes the matrices and ideals, not the calculation itself.

This final line is therefore not a new assumption but a bookkeeping identity: once the compact datum is fixed, the paper's data are a finite family of matrices, ideals, and divisor classes, and every spectrum, coupling, and flux count is read from them.

For a direct hand check one may start from a divisor basis $D_1, \dots, D_\rho$ on B_3 and lift it to $\widehat{Y}_4$. The intersection ring gives numbers

$$\kappa_{abcd} = D_a D_b D_c D_d, \qquad \kappa_{ijab} = E_i E_j \pi^* D_a \pi^* D_b, \tag{G13}$$

and the Cartan block is recovered by pushing forward the second expression to the gauge divisor. The conditions used in the paper are then nothing more than linear equations in these entries:

$$G_4 \pi^* D_a \pi^* D_b = 0, \qquad G_4 S_0 \pi^* D_a = 0, \qquad G_4 E_i \pi^* D_a = 0 \tag{G14}$$

whenever the last equation is required by the chosen non-abelian gauge symmetry. If a Shioda class σ_A is present, the abelian charge of a surface S_R is the single integer $S_R \sigma_A$. This is why the charge table and the chirality table are checked in the same pass through the Chow ring.

The stabilisation part is recorded in the same finite language. A period vector $\Pi(z)$ and a flux vector N give

$$W_{\mathrm{flux}}(z) = N \cdot \Pi(z), \qquad D_i W_{\mathrm{flux}}(z) = 0. \tag{G15}$$

At a solution z_*, the Hessian block that is tested in the paper is

$$H_{i\bar{j}} = \partial_i \partial_{\bar{j}} \left(e^K K^{a\bar{b}} D_a W \overline{D_b W} \right)_{z=z_*}. \tag{G16}$$

The model is kept only when this matrix has the required sign on the physical directions and when the resulting value of W_0 is compatible with the displayed non-perturbative terms. Thus the metric problem is not detached from the spectrum problem: the same flux integer determines the chirality, the superpotential, and the tadpole cost.

For the local Yukawa calculation the ideal $I_p = (F_1, F_2, F_3)$ is reduced with respect to a monomial order chosen once in the local patch. If $\mathcal{B}$ is the resulting basis of $\mathcal{R}_p$, multiplication by a zero-mode representative ψ_i is represented by a finite matrix M_{ψ_i}. The cubic map is then read from

$$M_{ijk} = \mathrm{Tr}_{\mathcal{R}_p} \left(M_{\psi_i} M_{\psi_j} M_{\psi_k} M_J^{-1} \right), \tag{G17}$$

where $J = \det(\partial F_a / \partial x_b)$ is the local Jacobian class whenever it is invertible in the residue pairing. This formula is the same for the $SU(5)$, $SO(10)$, Pati–Salam, and E_6 examples. Only the ideal and the chosen weight surfaces change.

The last consistency check is integrality. The shifted condition is written as

$$G_4 = g - \frac{1}{2} c_2(\widehat{Y}_4), \qquad g \in H^4(\widehat{Y}_4, \mathbb{Z}), \tag{G18}$$

so every matter index is checked as

$$\int_{S_R} G_4 = \int_{S_R} g - \frac{1}{2} \int_{S_R} c_2(\widehat{Y}_4) \in \mathbb{Z}. \tag{G19}$$

When the second term is half-integral, the first term must have the matching parity. The Smith normal form of the full constraint matrix records this parity together with hypercharge masslessness and the prescribed generation number. This prevents a spectrum from being accepted by a visual diagram or by an approximate scan alone.

Consequently the paper closes with one reproducible prescription. Fix the compact datum, compute the Chow ring, impose the flux equations, count the lattice points inside the tadpole region, push the surviving classes through the matter surfaces, and evaluate the local residue rings. If two entries differ only by a chamber automorphism, keep one representative. If a proposed entry fails integrality, transversality, tadpole positivity, or residue finiteness, discard it. The resulting list is finite for the fixed compact datum and each entry carries its spectrum, charges, vector-like part, coupling data, and stabilisation tests in the same notation used above.

In this final form the output of the paper is a finite table equipped with maps, not a disconnected catalogue. For every surviving representative $[n] \in \mathcal{F}/\!\sim$, the stored row is

$$[n] \longmapsto \big(G_4(n), \{\chi_R(n)\}_R, \{q_A(R)\}_{A,R}, \{Y_{ijk}(n)\}, W_0(n) \big). \tag{G20}$$

The same row also records the residual tadpole

$$N_{D3}(n) = \frac{\chi(\widehat{Y}_4)}{24} - \frac{1}{2} \int_{\widehat{Y}_4} G_4(n) \wedge G_4(n), \tag{G21}$$

which must be a non-negative integer. This last integer is the simplest independent check on the calculation: if it is negative, fractional, or inconsistent with the parity condition, the flux point is removed before any phenomenological interpretation is made.